DEVELOPMENT OF A NON-LIVING MODEL SYSTEM FOR CELL MEMBRANES AND INVESTIGATION OF ITS MECHANICAL AND TRIBOLOGICAL PROPERTIES

BY

TOOBA SHOAIB

THESIS

Submitted in partial fulfillment of the requirements
for the degree of Master of Science in Materials Science and Engineering
in the Graduate College of the
University of Illinois at Urbana-Champaign, 2016

Urbana, Illinois

Advisers:

Professor John R. Abelson
Professor Rosa M. Espinosa-Marzal

ABSTRACT

While our exposure to nanomaterials (NMs) has increased with advancements in nanotechnology, understanding harmful effects of such materials on humans is still wanting. Here we have proposed and developed a non-living model system for cell membranes which is suitable for elucidating interactions between NMs and living cells. In contrast to existing model systems for cell membranes, PAAm hydrogel was used as soft support for the lipid. Grafting of lipid with PAAm was achieved through layer by layer deposition of alternating poly(allylamine hydrochloride) (PAH)and poly(sodium 4-styrenesulfonate) (PSS) polyelectrolyte multilayers (PEM). Single step bilayer formation was observed under QCM on the PAAm-PEM support owing to high electrostatic interactions between the PEM and lipid vesicles with frequency and dissipation changes of ~-30 Hz and ~0.8×10^{-6}, respectively. It is also shown that the PEM architecture is robust and reproducible on gels of different elastic modulus. AFM images confirm bilayer formation on top of PAAm-PEM supports with uniform bilayer patches of ~ 0.5 μm. AFM indentation experiments show significant differences in the elastic modulus and adhesion forces for systems with soft underlying supports compared to systems having a hard substrate. The physiological relevance of the developed system is clear from its mechanical characterization via AFM, where the system undergoes considerable deformation *before* and *after* bilayer rupture. This behavior is similar to behavior of real cells, in which deformation of cytoskeleton is dominant over that of the cell membrane. The model cell membrane system was also used to study shear forces at the interface of the lipid bilayer on hydrogel, which gave insights into the frictional behavior of the system and its mechanical interactions with nanoprobes.

ACKNOWLEDGEMENTS

I would like to thank my advisers Prof. Rosa M. Espinosa-Marzal and Prof. John R. Abelson for giving me the opportunity to work on this project and guiding me through the project. I'm also grateful to my lab members at SIEN, especially Dr. Prathima Nalam for her help and guidance.

I want to acknowledge IGB for facilitating FRAP experiments.

I'm thankful to the Fulbright Program and U.S. Department of State funding my masters at UIUC.

Lastly, I would like to thank my parents for always supporting me through my academic goals.

TABLE OF CONTENTS

CHAPTER 1
INTRODUCTION

"There is plenty of room at the bottom"
-Richard P Feynman (1959, Caltech)

Over a decade, nanotechnology has opened innumerate exciting avenues of research for the scientific community. While these advancements bring useful solutions to the technological world, they carry certain risks. For instance, it has been established that nanoparticles can easily penetrate and absorb into living organisms [1], [2]. Furthermore, the likelihood of human exposure to nanomaterials has also increased with progress in the research and applications of nanotechnology. Since behavior of nanomaterials is different from bulk materials and little has been thoroughly investigated about their toxicological effects on the environment and living beings, knowledge of the deleterious effects that may arise when living cells are exposed to such materials is still wanting. To completely comprehend the effects of NMs on living cells, a thorough understanding is needed regarding the interactions between living cells and nanoparticles and mechanisms that lead to the adhesion and uptake of, and damage by, these particles.

1.1 DEVELOPMENT OF MODEL CELL MEMBRANE SYSTEM

Cell membranes are the first components of living cells that interact with foreign bodies or exogenous agents. They are highly selective, permeable biological interfaces that separate interior of living cells and outside environment. They maintain required environment for the interior cell by regulating molecular transport across the membrane, provide mechanical stability to the living cell and an interface for interactions with external entities. They are also dynamic 2D structures in the sense that they can undergo changes as a response to the environment as shown by various biological phenomena such as endocytosis, exocytosis and cell signaling. They are essentially composed of a lipid bilayer embedded

with proteins and polysaccharides which regulate the flow of nutrients, wastes etc. in and out of the cell [3][4]. A lipid molecule consists of a polar “head” group and a hydrophobic acyl chain termed as the “tail” group. Lipid molecules form a bilayer by orienting in a tail-to-tail fashion, where the polar head groups are in contact with the aqueous environment while hydrophobic chains are shielded from it.

Real cell membranes are complex in terms of their composition, structure and environment. It is not only difficult to separately study the effects of a certain stimulus or response of a particular membrane component in real systems, but it is also challenging since real cells are highly susceptible to denaturation and cell death in the testing environments. Hence to investigate various phenomena such as interactions between cell and solutes, cell fusion, cell differentiation, and cell damage among others, model systems for cell membranes have been used as they allow systematic studies of multitude of parameters [5][6].

Supported lipid bilayers (SLBs) are a common model system used for studying membrane formation and behavior[7][8][9][10], membrane cytotoxicity [1][11][12][13] and effect of solute additives [14]. In SLBs, the lipid bilayer is usually adsorbed onto a hard impermeable substrate [15][16] [17]. The formation of this bilayer on a substrate has been achieved via a number of techniques [18]–[20][21], but vesicle fusion and Langmuir Blodgett deposition has been the most extensively explored methods [22]. In the former, lipid vesicles are adsorbed onto a substrate with subsequent rupture and formation of a bilayer[23][24]. This process is highly dependent on the substrate-lipid interactions, nature of the lipid [22] [25], vesicles size[23] and concentration [16], pH of solution [15] and temperature [23]. In Langmuir Blodgett method, lipid molecules are directly adsorbed on the substrate, one monolayer after the other to form a bilayer [17].

However, studies have pointed out several limitations of SLB model. First of all, high adhesion between the lipid bilayer and substrate leads to a decreased lateral mobility of the lipid bilayer, in contrast to the 2D fluid nature of living cells membranes[26]. Since the investigated lipid bilayers are just a few nanometers in height, the proteins embedded into the lipid bilayer usually lack mobility owing to their strong interaction with the substrate, which differs from the behavior of the proteins embedded in living cell membranes [27][28]. Besides, the diffusion path for solutes is much shorter in the SLB model compared to that in real cells. We also note that the mechanical response of the hard (elastic) support for SLBs (usually an oxide such as silica) differs from the viscoelastic behavior of living cells [29], and hence, they both affect the bendability, stretching and tension of the cell membrane in a very different fashion. This difference in mechanical properties is bound to affect the accuracy and depth of interaction studies such as adhesion and detachment of macromolecules, and nanoparticles, and hence it provides incomplete and incorrect insights.

To overcome and partially solve the limitations mentioned above, it is proposed that a polymer film can be inserted between the lipid bilayer and the solid substrate[30][31]. This polymer layer could provide the polymer-supported lipid bilayer a) with certain lateral mobility, b) a spacer between the lipid bilayer and the solid substrate, hence minimizing the solid substrate effects and increasing the contact area for embedded macromolecules, and c) a longer diffusion path length for solutes. To date, the investigated supports have been polyelectrolyte multilayers (PEMs) with a thickness of a few tens of nanometers, which is still much smaller than the size of real cells [32][33]. Additionally, these studies were only limited to the formation of a lipid bilayer on PEMs and did not investigate the properties of the system.

Hydrogels are cross-linked polymer networks that contain large amounts of water [31]. They can respond to changes in pH [34], temperature[35], and ionic strength. Their biocompatibility and hydrophilic properties have made them favorable for applications in biological and clinical fields. Furthermore, the polymer volume fraction in these gels can be used to easily tune the (visco)elastic behavior, enabling simulations of a large variety of cell mechanical properties, which is an advantage compared to other polymer films. Although lipid bilayers have been absorbed on microgel particles before [36], [37], to the best of our knowledge studies of the formation of lipid bilayers on planar hydrogels –which are needed for our further studies- have not been reported yet.

Here we present a novel cell membrane model consisting of a hydrogel-supported lipid bilayer. The hydrogel, polyacrylamide (PAAm) has a tunable height i.e. 4-200 μm in this work. A phospholipid bilayer is deposited on the hydrogel via a PEMs graft. This grafting method is expected to increase the adsorption of the phospholipid on the hydrogel while also facilitating the formation of a bilayer on the soft support through vesicle fusion. The choice of materials enables control of mechanical properties such as stiffness of the system hence further enhancing its use as a model system for real cell membranes.

The system is partly assembled and characterized in-situ by Quartz Crystal Microbalance (QCM) to ascertain formation of a bilayer and study the formation kinetics. Furthermore, Transmission Interferometer Adsorption Sensor (TInAS), Fourier-Transform Infrared Spectroscopy (FT-IR) and Fluorescence Recovery after Photobleaching (FRAP) are used to additionally characterize the system. Atomic Force Microscopy (AFM) is employed to image the surface of the hydrogel-supported membrane, and AFM force spectroscopy to perform nanomechanical studies of the system and deduce mechanical properties arising from such an assembly.

This approach utilizes convenient polymer synthesis and self-assembly processes, yet, it renders a high level of customization and tunability of the proposed system. Owing to various control parameters

involved, it enables to perform a number of systematic studies on membrane-nanoparticle interactions, consequently assisting in the design of safe and/ or biocompatible nanomaterials.

1.2 HYPOTHESIS AND APPROACH

Since biology of real cells is quite complex with a plethora of processes and properties involved, it has been more convenient to study behavior of real cell membranes by biomimetic systems. These model systems not only provide a convenient method of performing analysis but have also provided us with a way to separately study individual aspects of cell membranes [38].

As this project has its essence in studying the ***contribution of the membrane mechanical properties on the uptake of nanomaterials (NMs) by cells***, Figure 1a is an illustration of what might this uptake process look like. Little is known about the mechanisms underlying cell damage by NMs but it has been suggested contact between NMs and the cell membrane, followed by engulfing by the cell membrane (facilitated by ligand, receptors or other entities on the membranes) is the process behind cell damage. For a nanoparticle to be wrapped by a cell membrane, the total adhesion energy must overcome the resistive forces (the penalty) associated ***with membrane tension and bending, and cell deformation***, and hence this thermodynamically favorable process should be significantly influenced by the mechanical properties of cells and cell membranes. NMs are very reactive due to their high surface-to-volume ratio. Harmful genetic effects have been reported for some manufactured NMs on cells [39]. Our interest is to elucidate the first stages of cell contact and penetration; the fate of the NMs inside cells is out of the scope of this work.

When NMs are exposed to biological fluids, the proteins and biomolecules present therein adsorb onto the nanoparticles' surface forming a biomolecular corona as shown in figure 1a [4]. The corona determines the particle interactions with biological systems. Considering the simple illustration in Figure 1a, we can see that ***the viscoelasticity of the near-surface cell region*** could determine the fate of the nanoparticle. The near-surface cell region is composed of membrane, actin cortex and linkers –in animal cells, while the designed system in this work is simplified by lipid bilayer, hydrogel and PEM grafting layer.

It is our hypothesis that there might be a strain energy contribution to the overall NM-cell membrane interaction, which will depend on the (non-linear) viscoelastic behavior of the cell in question. A thermodynamic approach of the uptake of a nanoparticle can be described by

$$\Delta G_{bind} = \Delta E_{Strain} + \Delta G_{\gamma} - T\Delta S$$

where ΔG_{bind} is the free energy released by specific (e.g. receptor-ligand interactions) and non-specific (electrostatic, hydrophobic, and depletion attraction), which promotes nanoparticle wrapping, ΔE_{Strain} is the strain energy required for the deformation of the near-surface cell region (until rupture), and ΔG_{γ}considers the contribution of the surface energy, which should be relevant due to the large curvature of the nanoparticle, and ΔS is the entropy loss of the bound receptors.

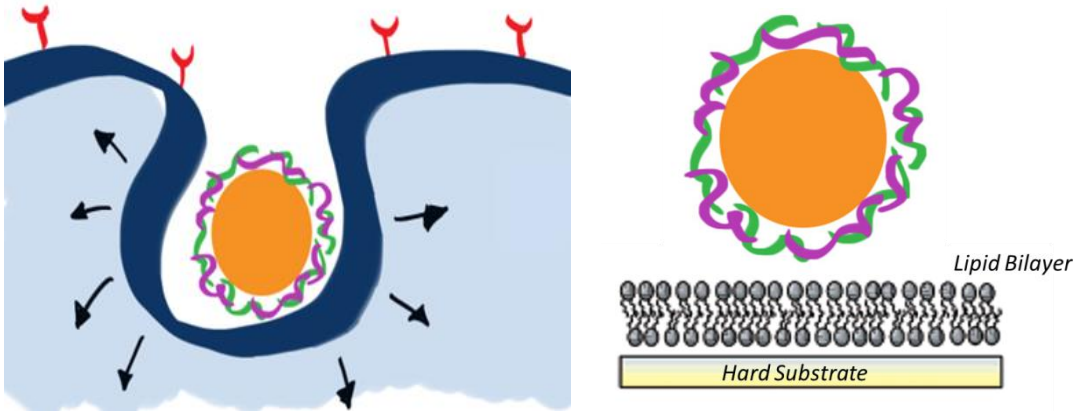

Figure 1: a) An illustration of NP with protein corona around penetrating into a living cell. The cell membrane (in dark blue) bends upon contact with NP b) Classical SLB model system with a lipid bilayer on top of a hard substrate. The NP on top highlights inherent limitations of this model system (part of figure adapted from [40]**).**

Figure 1b shows a common model system which is used to study cell membranes, SLBs on hard substrate, as mentioned in the previous section. If we think about studying an interaction of the nature as illustrated in Figure 1a., the physiological incorrectness of this model is evident, since not only there are high substrate effects but the membrane lacks the ability to bend upon contact with a nanoparticle (NP) and/or engulf it. This ability to bend and deform of the cell membrane is the key aspect of our hypothesis and study, hence our approach utilizes a tunable substrate beneath the cell membrane, which enables us to customize mechanical properties and study the effects of their variations. This is achieved by using PAAm hydrogel with modulus in the range of 2-9 kPa as the polymer cushion on top of which alternating layers of polyelectrolytes (PEMs) are deposited. Their function is to provide a charged surface for the lipid molecules to adsorb on and adhere to the neutral polyacrylamide gel surface. The final layer is the bilayer itself and is deposited from a buffered liposome solution in this work.

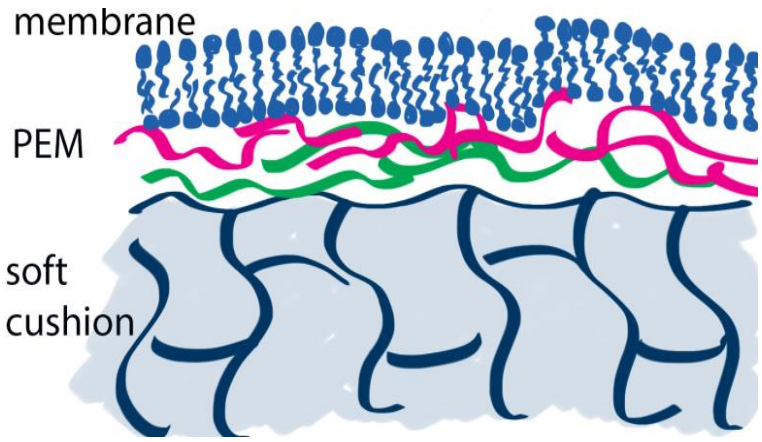

Figure 2: Proposed model system for mimicking a real cell membrane. A tunable, crosslinked polymer gel (blue) with thickness in the range of 4-200 µm is used as the support for lipid bilayer (purple), 5 to 7 nm. The grafting is achieved via PEMs (orange and green) having a total thickness of 10-20 nm.

The purpose of this project is to first develop stratified system as described and tune the materials and methods to obtain an optimized model system for cell membranes. The next portion of this work is to investigate the interactions of nanoprobes with different tip chemistries with this model system as a method of simulating nanoparticle-cell membrane interactions. These interactions will be studied via nanoindenations and friction measurements. It is expected that a better understanding of the mechanisms behind cell-nanoparticle interactions will help in understanding in vivo processes such as nanoparticle wrapping and ingestion by cells or the biolubrication properties associated with lipids. The study will also help in the design of more functional biomaterials.

CHAPTER 2
MATERIALS AND METHODS

2.1 MATERIALS

For the preparation of polyacrylamide hydrogel, 40% (w/v) acrylamide (AAm) stock solution, 2% (w/v) bis-acrylamide (Bis-AAm) stock solution, tetramethylethylenediamine (TEMED) and 10% (w/v) ammonium persulfate (APS) were obtained from Sigma Aldrich and were used as it. Dichlorodimethylsilane (DCDMS) was used to pretreat the 25 × 75-mm glass slides involved in fabricating the hydrogels on Quartz Crystal Microbalance (QCM) gold sensors. Deionized (DI) water was used to prepare all solutions for synthesizing the gels.

Polyelectrolyte multilayers were deposited from solutions of poly(sodium 4-styrenesulfonate) solution (PSS, 70 kDa), poly(allylamine hydrochloride) (PAH, 17.5 kDa) and sodium chloride which were obtained from Sigma Aldrich. Milli-Q water (Milli-Q, 18.2MΩ, Millpore, USA) was used for making the polyelectrolyte solutions.

For lipid vesicles, suspensions of egg phosphatidycholine (EggPC, 1mg/ml in chloroform), 1-palmitoyl-2-oleoyl-sn-glycerol-3-phosphocholine (POPC, 1mg/ml in chloroform) and 1-palmitoyl-2-oleoyl-sn-glycero-3-phospho-L-serine (sodium salt) (POPS, 1mg/ml in chloroform) were obtained from Avanti Polar Lipids, ME, USA. Texas Red 1, 2-dihexadecanoyl-*sn*-glycero-3-phosphoethanolamine, triethylammonium salt (Texas Red® DHPE) (Thermofisher, USA) was added in 1mol% in all lipid solutions. Solutions of 10mM Tris (Sigma Aldrich) and 10mM HEPES (Sigma Aldrich) having 100mM NaCl were used as buffers. Milli-Q water was used for all the lipid solutions. Unless indicated, water means Milli-Q water.

2.2 METHODS

2.2.1 Polyacrylamide (PAAm) Hydrogels

The protocol for preparing polyacrylamide gels was adapted from literature [41], with modifications to cater for change of substrates. Selected substrates for the hydrogels were glass coverslips

(25 mm in diameter) for FTIR and gold QCM crystals. For AFM imaging, hydrogels grafted to gold QCM crystals were used. For AFM indentations hydrogels grafted to coverslips were used. The choice of substrates will be mentioned accordingly.

A mixture of AAm and Bis-AAm in DI water was degassed under strong vacuum for 15 min to remove the dissolved oxygen. The amounts of monomer and crosslinker were varied to obtain different elastic moduli in the range of 2 to 9 kPa. After degassing, APS (1/100 of total volume) and TEMED (1/1000 of total volume) were added to the mixture and the solution was vortexed for 30 seconds. Immediately after, a fixed amount of this solution was pipetted on to functionalized glass slide surface (5 μL for QCM sensors and 20 μL on coverslips) and was then sandwiched by slowly placing the coverslip or QCM sensor on top of the solution. The hydrogel was allowed to polymerize for 30-40 minutes, which is the time that it took for gelation to take place in the polymer solution that remained in the flask.

After polymerization, the coverslips and QCM sensor were removed slowly through a sliding motion from the glass slides. Coverslips were rinsed with DI water to remove unpolymerized acrylamide. QCM sensors were mounted on the fluid cell immediately and then rinsed with MilliQ water under a flow of 50 μL/minute till a constant baseline could be obtained in QCM which typically took 1 to 2 hours. Hydrogels with varying modulus of elasticity were obtained by changing amounts of acrylamide (AAm), and the cross-linker, Bis-AAm. The prepared gels were tested with Atomic Force Microscopy (AFM) for modulus measurements which will discussed in AFM section.

2.2.2 Preparation of Lipid vesicles

Small unilamellar lipid vesicles were prepared by following the protocols in reference [42]. It should be mentioned here that the protocol remained same for all lipids used i.e. EggPC and POPS. However, the two lipids were prepared in both 10mM Tris 100mM NaCl pH 8.0 and 10mM HEPES 100mM NaCl pH 6.2 buffer, hence in this section instead of the type of buffer, just the term “buffer” will be used. A lipid solution of 10mg in chloroform was transferred to a round bottom flask along with 180 μL (1 mol%) of the dye. The lipid was dried onto the walls of the flask by continuously rotating the flask under high vacuum for 4-6 hours to ensure complete removal of solvents. After drying, a 10 mL buffer solution was added to the round bottom flask under constant supply of nitrogen, to avoid lipid contact with oxygen. Lipid was resuspended in the buffer by vortexing the solution for 30 minutes. The solution was then sonicated to clarity using 1/8” microtip of Branson probe sonicator (Fisher Scientific,

USA) to obtain lipid vesicles. The sonication was done in a centrifuge tube inside an ice bath in 5s pulses separated by 5s cooling period with an amplitude of 35%. The sonication time was 1.5 hours.

The clear (tinted pink due to the dye) vesicle suspension was spun at 150,000 × g for 4.5 h in ultracentrifuge (Beckman Coulter, USA) to separate small vesicles from lipid structures. Two fractions formed after centrifuge and the upper fraction was used in all experiments. To characterize the vesicle size and zeta potential using Dynamic Light Scattering (DLS) Zeta Sizer Nano ZS90 (Malvern Instruments, USA).The refractive index and light absorption were assumed to be 1.47 and 0.1, respectively.

The upper fraction having 1mg/ml of lipid was stored separately under nitrogen at 4ºC. This solution was diluted prior to use in by adding 9 ml of buffer solution to 1 ml of lipid solution in order to get a concentration of 0.1 mg/ml of lipid.

2.2.3 Quartz crystal microbalance (QCM)

For the proposed model system, QCM was used to partly fabricate the system as well as to monitor the formation of supported lipid bilayer (SLB) in situ.

Two types of QCM sensors were used, Gold and Silica, depending on the system that was being fabricated. QCM experiments were done for three systems: a lipid bilayer on Silica sensor, a lipid bilayer on PEMs deposited on Silica sensor, a lipid bilayer on hydrogel with PEMs on top of a Gold sensor. For most experiments, a PEM system having 5 layers of polyelectrolytes PAH $(PSS\text{-}PAH)_2$ was used for. But to determine the dependence of PEM architecture and adsorption behavior on number of layers of the PEMs, and also to observe if the polymers were going inside hydrogel pores, PEM system having 9 layers $PAH(PSS\text{-}PAH)_4$ was also deposited on PAAm gel. Similarly, PAAm gels of different moduli and PAH of different chain lengths were also used to study corresponding effects. These experiments will be clearly mentioned along with the resulting QCM plots in results section.

All QCM sensors were cleaned prior to use. Gold sensors were first exposed to UV ozone for 10 min then immersed for 5 minutes in a 1:1:5 solution of hydrogen peroxide (30%), ammonia hydroxide (25%) and water which was heated to 75 ºC. The sensors were immediately rinsed with water and dried with nitrogen after the treatment and further exposed to UV for 20 minutes. For Silica QCM sensors exposure to UV ozone was done for 10 minutes after which sonication was carried out in Sodium dodecyl sulfate (SDS) solution (2% w/v) for 30 minutes. After sonication in SDS, the sensors were immediately rinsed with water and dried with nitrogen. A final exposure to UV zone was done for 10 minutes. All QCM crystals were immediately used after cleaning procedures. The QCM cells and tubing were also

cleaned before each experiment by running SDS (2% w/v) through them for 10 minutes and then water for 30 minutes at a flow rate of 300 μL/min.

For depositing PEMs, polyelectrolyte solutions were first prepared in bulk by dissolving PAH and PSS in water to make a concentration of 2mg/mL of the polymers with 500mM of NaCl. The solutions were sonicated at 50 ℃ overnight and then stored in at 4℃. Before each used, the solutions were filtered using a 0.2 μm nylon steriile syringe filter and then degassed and sonicated for 30 minutes.

PAAm gels were deposited ex-situ on the gold sensors as described previously. After mounting and equilibration in the QCM cell under water, the QCM system was tuned to the resonant frequency of hydrogel on gold sensor. Silica sensors were mounted in the QCM directly after cleaning and resonant frequencies were recorded. The baseline was obtained in water at a flow rate of 50 μL/min for all experiments. After acquiring a baseline, PEMs were grafted on the hydrogels or directly on Silica sensors by the layer-by-layer deposition method. PAH solution was introduced in the system and allowed to run for 15 to 20 minutes or till equilibrium (when the frequency and dissipation reach a constant value). Rinsing was carried out for 10 minutes or till equilibrium, to wash away weakly adsorbed polyelectrolyte, before flowing in PSS solution. The PEMs system was deposited in this fashion till 5 or 9 layers of PEMs had formed.

Lipid vesicle adsorption and bilayer formation was studied on bare Silica sensors, Silica crystals with PEMs and on PAAm supported PEMs. Before introducing the vesicles solutions, a baseline was obtained in buffer solution. For systems with PEM and PAAm supported PEMs baseline was obtained in buffer with an added 25 μM of $CaCl_2$. The addition of Ca+2 was done to enhance adsorption of lipid vesicles on hydrogels and PEMs [43]. Afterwards, the diluted lipid solution in the same buffer was flown in. After reaching equilibrium, again buffer solution was passed to rinse away any weakly adsorbed lipid.

2.2.4 Fourier Transform Infrared Spectroscopy (FTIR)

For determining the adsorption of lipids outside of QCM and on other substrates than QCM crystals, FTIR was carried out using FT-IR PerkinElmer, USA and spectra was recorded within the range of 400 cm^{-1} to 4000 cm^{-1}. PAAm hydrogels were fabricated on glass coverslips as described previously and the coverslips were immersed in polyelectrolyte solutions of PAH and PSS, 2 mg/mL 500 mM NaCl each, alternating the positive and negative polyelectrolytes and rinsing twice with water in between. The immersion times were 15 minutes for both polyelectrolyte depositions and rinsing. A total of 5 layers were deposited starting and ending in PAH.

After the PEM formation, the samples were immersed in buffer with 25 μM $CaCl_2$ for 30 minutes. Then, the samples were immersed in 1 mg/mL solution of lipid vesicles with 25 μM $CaCl_2$ for two hours. A longer time and higher concentration was adapted for the lipid to absorb to compensate for lack of flow conditions in immersion technique. After incubation in lipid solution, the samples were rinsed in buffer to remove weakly adsorbed lipid vesicles. The samples were scooped from the coverslip and placed on the ATR crystal for measuring the spectra. The IR spectrum corresponds to ~1-2 μm in depth and therefore it gives the superposed spectra of hydrogels and all adsorbed layers.

2.2.5 Fluorescence Recovery after Photobleaching (FRAP)

For confirming formation of a bilayer on coverslip samples, FRAP was performed with LSM 710 Confocal Microscope (Zeiss, Germany) using 594 laser at 100% power output (5mW). Photobleaching was done for 3 seconds prior to obtaining recovery images at a sampling rate of every 2 seconds for 20 minutes.

Two types of samples were made: lipid bilayer on glass coverslip and lipid bilayer on PAAm-PEMs i.e. full stratified system. For samples with PAAm gels, 25 mm coverslips were treated with 0.1M NaOH, 3-Aminopropyltriethoxysilane (APES) and 0.5% (v/v) glutaraldehyde in phosphate-buffered saline (PBS) to enhance grafting to the glass surface.

After deposition of PEMs, samples were incubated in buffer solution for 30 minutes after which 10μL droplet of lipid solution, 1mg/mL, was placed on a plastic petri dish having adhesive spacer strips, on which the samples were placed face down. After 2 hours, the inside of petri dish was rinsed with buffer, three times, with ten minute incubation periods. Steps starting with incubation in buffer and onwards were adapted for preparing lipid bilayers on glass.

2.2.6 Atomic Force Microscopy (AFM)

AFM imaging and indentation experiments were carried out with JPK Nanowizard Ultra A. AFM sharptips (0.3 N/m, Mikromasch,Estonia) were used for imaging lipid bilayer on Silica sensors, PEM on Silica sensors, PAAm on coverslips and SLBs on PEMs and SLBs on PAAm supported PEMs. All imaging was done in contact mode. For systems with the bilayer on top, imaging was done in buffer solution while all other systems were imaged in water.

For modulus measurements of PAAm and PEMs, a colloid probe method was used to reduce local stresses and error in measurements. Indentation was also done on systems with SLBs using sharptips to observe the characteristic bilayer rupture event.

Friction measurements were performed with three different tips: 1) blunt silica tips (sharptips, 0,3 N/m, Mikromasch, Estonia, annealed for 2 hours at 1050 °C) 2) Silica Colloid tip (0.48 N/m, Nova) 3) Biolevers (0.3N/m, Au tip, Mikromasch, Estonia).

All measurements reported were conducted at a scan speed of 1µm/s and 10µm scan length. All samples for friction measurements were prepared as described in the FTIR section.

2.2.6.1 Imaging

AFM imaging was done on samples prepared in QCM. Three systems were imaged: Lipid bilayer on Silica sensor, PAAm supported PEMs on Silica sensor and SLB on PAAm supported PEMs. The samples were prepared in QCM to relate adsorption and PEMs and formation of bilayer with the imaging results. After fabricating in QCM, the sensors were placed on glass slides and fixed via adhesive tape.

2.2.6.2 Nanoindentation

Modulus measurements for three systems: PAAm, PAAm with PEMs on top and only PEMs were carried out. Tipless cantilevers (0.3N/m, Mikromasch, Estonia) were first calibrated to determine the normal spring constant by the thermal noise method after which a colloidal sphere around 10 μm in diameter was glued to the tip of the cantilever.

The sensitivity of the cantilever was also determined by a normal force measurement on a glass slide immersed in water. Since sensitivity can vary depending on the day of experiments, this measurement was carried out before every experiment. In AFM indentation experiments, an indenting probe is moved towards the sample and cantilever deflection versus the probe displacement is recorded. After the set force is reached, AFM probe is retracted and the retraction curve of cantilever deflection versus the probe displacement is acquired.

After PAAm hydrogel was grafted on the coverslip, the coverslip was attached to a freshly cleaned glass slide using carbon adhesive tape and placed on the AFM sample holder. A few droplets of water were deposited on the top of the hydrogel to avoid drying in air. A 5μm force distance was used to pull out the colloid sphere after each indentation due to high adhesion between the systems and colloidal sphere. The maximum loads were 20nN and the approaching speed was 5 $\mu m/s$. The elastic modulus was determined from the force-distance curve upon approach by using Hertz contact model.

For systems with the SLBs, sharptips (0.3 N/m, Mikromasch, Estonia) were used to acquire force curves. This was done to minimize contact area and hence determine the presence of bilayer by observing characteristic rupture of bilayer during the extend portion of the force curves. After preparation of samples in QCM, the sensors were carefully taken out of the QCM cells and quickly mounted on glass slides and fixed via adhesive tape. Extra precaution was taken to keep the sensors with the SLBs on top

from drying out since it would cause the bilayer to be lost. To observe the bilayer ruptures, approach speeds of 300 nm/s, 1 $\mu m/s$ and 1.5 $\mu m/s$ were used. Higher approach speeds were used for systems

having PEMs or PAAm-PEMs underneath the bilayer, while for lipid bilayers on Silica 300 nm/s speed was used always. A force of 20 nN was applied for all force measurements. Rupture forces and penetration depths were recorded using the JPK data processing software.

CHAPTER 3
RESULTS AND DISCUSSION

Assembly and characterization of the proposed model system for cell membranes is shown through QCM, FTIR and AFM. Furthermore, nanomechanical studies of the developed system as well as other subsystems have been presented to provide a comparison of their mechanical behaviors.

3.1 ASSEMBLY OF THE MODEL CELL MEMBRANE SYSTEM

Prior to the fabrication of stratified systems the lipid bilayer formation was confirmed by QCM on silica-coated crystals. This confirmed the viability of lipid solutions and gave insights into the kinetics of a bilayer formation via deposition from liposome solution. Figure 3 shows a representative curve of bilayer formation on a silica QCM sensor. In QCM-D, changes in frequency are usually related to mass adsorbed. A dissipation change is associated with the dampening of oscillatory motion of sensors and refers to the viscoelastic properties of materials being adsorbed on the surface. Formation of a bilayer under QCM-D has been studied extensively [23], [44], [45]. On the silica substrates, it is well accepted that the vesicles first adsorb and above a critical concentration they fuse and form a bilayer [24]. Vesicle fusion is typically dominated by adhesion between vesicles and the substrate as adhesion enhances stress and leads to vesicle rupture and spreading. The observed mechanism is as follows: lipid vesicles adsorb on silica surface as intact structures, initially. Afterwards, mainly due to electrostatic forces between the substrate and vesicles and also between adjacent vesicles, the adsorbed vesicles rupture and fuse forming a bilayer. The exact mechanisms for spontaneous vesicle rupture and formation of a bilayer are still under debate and need further elucidation; however, electrostatic charges between surfaces and vesicles are

expected to be dominant in this process. In figure 3, vesicle adsorption is first seen as a downward shift in frequency of -64 Hz by which time a critical concentration of vesicles has been adsorbed on the surface to promote the “neighbor induced” vesicle rupturing. Hence, the frequency increases, indicating a loss of

mass attributed to the lost water upon rupturing of vesicles. After frequency stabilized, flowing in buffer rinsed out the weakly adsorbed lipid molecules, hence, a very small positive change in frequency was observed. The average change in frequency is -26 ± 2 Hz and has been reported as the characteristic

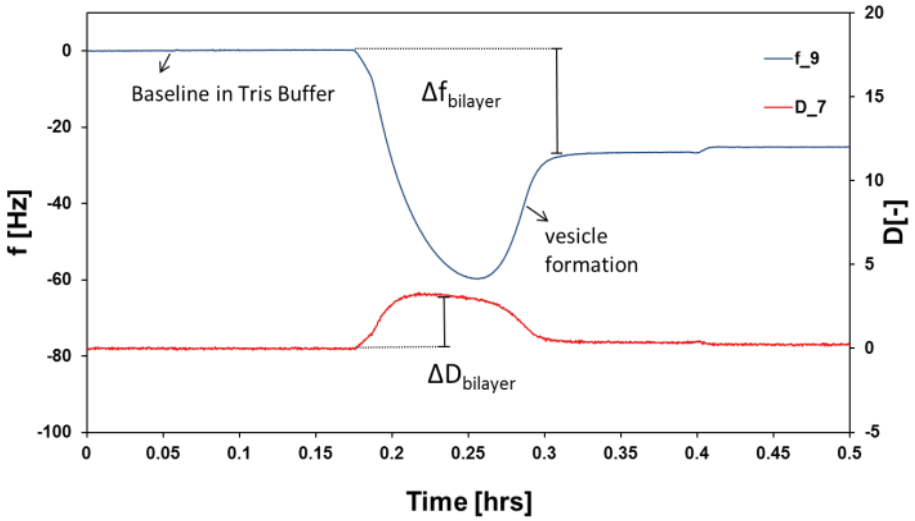

frequency change of bilayer formation on a silica support.

Figure 3: QCM plot of EggPC in 10mM Tris pH 8.0 100mM NaCl. Characteristic frequency well shows formation of a lipid bilayer on silica surface.

This frequency change is validated by Sauerbrey's equation, indicating the mass of lipid adsorbed on the sensor when an almost perfect bilayer covers the sensor surface (Sauerbrey predicts a bilayer thickness of 3.06 nm for $\Delta f = 26$ Hz). The red curve in Figure 3 plots changes in dissipation as a function of time. Dissipation increases while vesicles adsorb on the surface. As vesicles contain a large amount of water, making them viscoelastic in nature, this causes sufficient dampening of the oscillatory motion of the sensor. However, upon rupturing, dissipation goes back down to zero, indicating the presence of a very rigid layer of material on the sensor. This is due the very small thickness of lipid bilayer (3 - 5 nm) which itself is a rigid film.

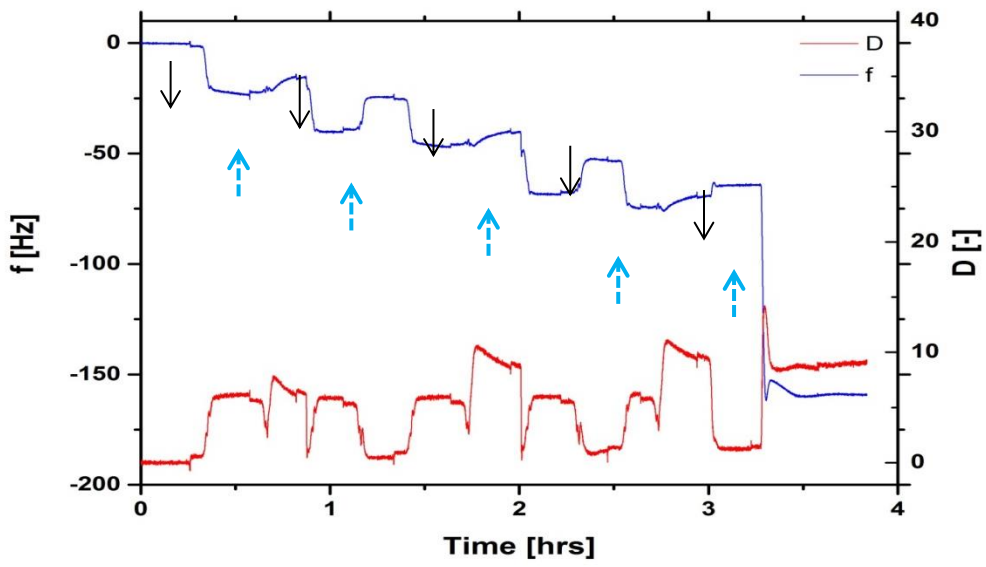

Figure 4: QCM-D plot showing PEM formation on Silica sensor and subsequent lipid adsorption. Black arrows: PEM injection (Starting with PAH and alternating); Blue arrows: rinsing steps.

Figure 4 shows representative QCM-D results for the formation of PAH-$(PSS\text{-}PAH)_2$ on silica sensor and subsequent lipid adsorption. Blue arrows indicate rinsing steps while black arrows indicate alternating polyelectrolyte injections starting with PAH. These sets of experiments revealed the PEM formation kinetics and adsorption behavior. The overall frequency decreases during layer-by-layer formation ($\Delta f \sim 61$ Hz), while the overall dissipation increases ($\Delta D \sim 3x10^{-6}$), although complex changes of both are observed at each single step. It should be noted here that QCM-D is sensitive to the total mass of the grafted layers to the sensor, including the mass of the associated solvent; hence the solvation of polyelectrolytes by water is also being recorded.

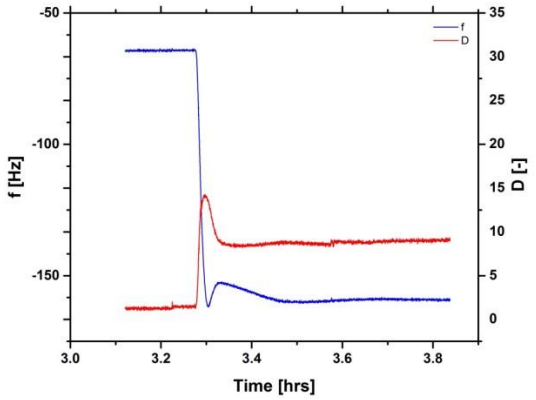

Figure 5: Zoomed portion of QCM-D plot showing the lipid adsorption on PEMs on a silica sensor. Baseline is obtained in 10mM Tris with 100 mM NaCl after which 0.1 mg/mL of EggPC in 10mM Tris is introduced. Shifts in frequency and dissipation indicate vesicle adsorption.

After adsorption of PEM layers, the sensors are equilibrated in buffer, 10mM Tris 100 mM NaCl with 25 μM $CaCl_2$, for ten minutes as shown in Figure 5. It has been previously shown that a complexation of the lipid layer with segments from the second last layer is possible [46][47] owing to entanglements between PAH and PSS chains. A relevant surface density of sulfates on the top layer is also possible for this system. Hence, vesicle adsorption was enhanced by adding small amounts of Ca2+to the vesicle solution [48]. Thus, it is likely that the calcium ions interact with PSS chains close to the PEM-solution interface and bridge the slightly negatively charged vesicles with the PEM that is grafted to the hydrogel. Presence of PSS at the surface was also confirmed by adhesion experiments done with AFM colloid probe indentations (See Supplementary Information).

After a stable baseline was acquired, the lipid solution was introduced (all lipid adsorptions were done in isotonic conditions). The decrease in frequency (Δf~ 160 Hz) indicates adsorption of lipid vesicles. An immediate spike is observed in the frequency plot and it is assumed that incomplete bilayer formation by smaller number of rupture events is taking place on the sensor surface. A very large increase in dissipation is seen initially ($\Delta D \sim 14 \times 10^{-6}$) which drops down to a final value of $\Delta D \sim 8 \times 10^{-6}$. Previous studies have shown that the large values of dissipation and frequency correspond to irreversible intact vesicle adsorption [49][48][47]. The results here however also indicate a partial rupture.

According to the Sauerbrey's equation, a total frequency decrease of 184 Hz would be expected for the adsorption of lipid vesicles (diameter = 64nm) on the smooth sensor surface. This is expected to be even higher if we consider the rough surface of PEM. Therefore, it can be reasoned that an incomplete

and imperfect bilayer forms on the sensor with a large number of intact vesicles. The adsorption of vesicles is very strong since rinsing with the buffer doesn't shift frequency or dissipation; this is expected since the vesicles have a net negative charge and will be tightly bound by the positively charged PAH at the pH of the experiment (pH of PAH solution is less than pKa value of PAH).

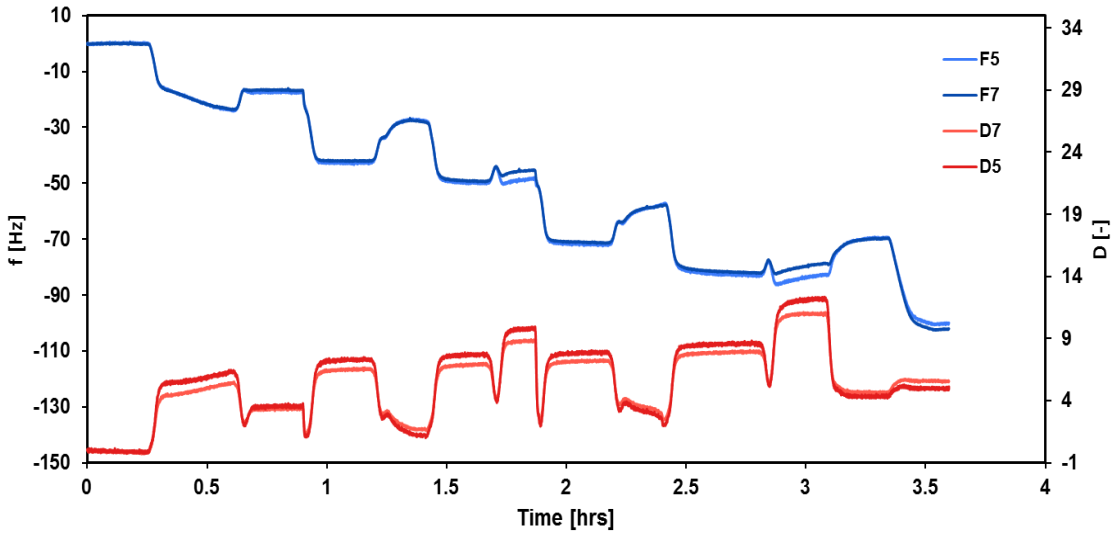

Figure 6: QCM-D plot of 7th and 5th harmonics during the assembly of the stratified system. PEM was adsorbed on a hydrogel-coated gold sensor with final step of lipid adsorption. A small frequency and dissipation shift is observed during the lipid adsorption indicating one-step bilayer formation.

Figure 6 shows a QCM-D plot of the assembly of the stratified system. During exposure of the hydrogel to PAH solution the frequency decreases and the dissipation increases, as expected from adsorption of polymer and increase in solution density (100 mM NaCl). During the rinsing step with water (blue arrows) after PAH exposure, the change of dissipation is complex: initially there is a fast decrease of dissipation that is attributed to the decrease in solution density; then the dissipation rapidly increases (while Δf decreases) which is attributed to the hydration of the polymers (swelling). During exposure to PSS solution, the frequency also decreases (negative change) and is higher than that observed for PAH which can be due to a higher molecular weight of PSS; in contrast a decrease in dissipation followed by an increase is observed. This complex change in dissipation is attributed to conformational changes of PSS upon adsorption. During polymer adsorption, we expect the polyelectrolyte to adsorb with the conformation in bulk and later to collapse at the surface, likely forming a "stiffer" polymer layer, explaining the decrease in dissipation.

PEM are usually soft or viscoelastic in nature due to the hydration water present in the film, and therefore the Sauerbrey expression often becomes invalid. For viscoelastic films, film mass and height can be deduced using the Voigt model [50], which assumes that the film has uniform thickness and density.

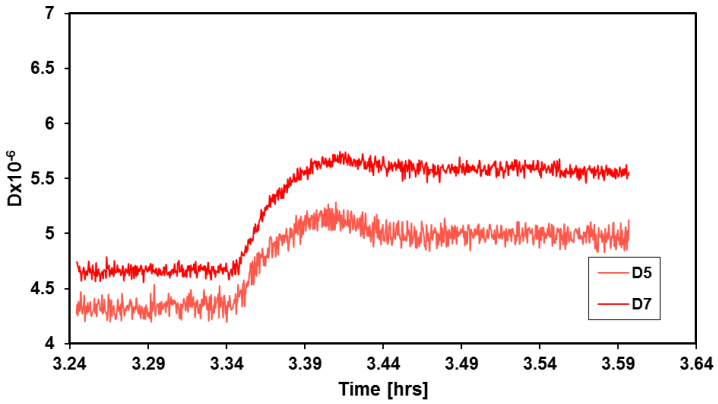

Figure 7: Dissipation of 5th and 7th harmonic during lipid adsorption on the PAAM-PEM system. The small change in dissipation predicts a one-step bilayer formation process.

The characteristic well in frequency described above (figure 3) for bilayer formation was not observed, which means that either the vesicles did not rupture at the interface or the rupture occurred immediately after adsorption. The change in frequency was ~-30±2 Hz and that of the dissipation was ~0.8x10-6 ± 0.2x10-6. A simple calculation demonstrates that the measured change in frequency is smaller than the expected change for full coverage of the sensors with vesicles having a size of 32 nm for this case: If one considers vesicles with 32 nm radius, a molar mass for the phospholipid equal to 770 g/mol and a surface area per phospholipid of ~0.85 nm^2, a full coverage of the QCM sensor with vesicles would lead to an adsorbed mass of 3.26 μg/cm2 or Δf~-184 Hz. This value includes the mass of water within the vesicle. Hence, a full coverage of the PEM-fluid interface with vesicles can be excluded. If the interface would be populated by vesicles, only a ~50% of the surface area would be covered by vesicles. However, results discussed later demonstrate that a larger percentage of the surface is covered with lipids and this is consistent with the formation of a discontinuous lipid bilayer on the PAAm-PEM. It should be noted again that the PEM-fluid interface is likely rough, which will enhance the surface area compared to flat surfaces. Therefore larger changes in frequency and dissipation are expected for a complete coverage of the hydrogel-supported and silica-supported PEMs with a lipid bilayer. From the results obtained in this work, it is plausible that a one-step bilayer formation is taking place on PAAm-PEM support due to the high interactions between PAH and lipid vesicles and presence of Ca^{+2} ions. The single step, bilayer

formation kinetics have been reported previously while studying effect of pH on vesicle rupture [49]. However, why intact vesicles reproducibly (90 ± 6 Hz) adsorb on silica-supported PEMs and do not undergo rupture is still not clear. While the surface heterogeneity in latter case might lead to additional stresses that facilitate fast vesicle rupture, however the exact causes are yet to be understood.

These results suggest that the driving force for the adsorption is the electrostatic interaction between the amino group in the PAH and the phosphate group in the lipid and successful bilayer formation occurs on PAAm-PEM as shown by the fast kinetics of adsorption and shifts in frequency and dissipation. The spontaneous lipid bilayer formation after vesicle adsorption involves a negative change in Gibbs free energy: an entropy gain results from the release of water molecules, whereas it involves an entropy loss for the surface-immobilized lipids and for the polymer chains at the interface; a variation in enthalpy results from the exchange of head group-water interactions in the vesicle by head group-substrate interactions for the bilayer; an increase in surface energy of the vesicles upon adsorption owing to additional stresses. The latter seems to determine whether the vesicles will deform (spread) and rupture or will remain stable at the interface. The gain in adhesion energy and resulting vesicle deformation results from the interactions with the substrate, which in this work is mainly of electrostatic nature. For attachment and rupture of the lipid vesicles, the affinity towards the support should be large enough – in our work very likely through electrostatic interactions between amino groups in PAH and phosphate in the lipid head - whereas spreading/rupture and formation of the continuous membrane requires local rearrangements of the lipids, for which lateral mobility of the lipids along the surface of the support is an essential condition. Strong short-range interactions (via hydrogen-bond) between zwitterionic lipids and PAH do not to promote vesicle spreading and rupture because vesicle deformation is negligible.

Apart from QCM measurements, IR spectroscopy and AFM topographical images (in liquid) were acquired to understand the formation and the stability of bilayers on soft PAAm-PEM systems. Figure 8 shows a section (1800 cm-1 to 800 cm-1) of the IR absorption spectrum for adsorbed lipid on PAAm-PEM. The spectrum shows peaks of PAAm: 1605 cm^{-1} (Amide II) due to the –NH2 bending vibration of the amide group and the –CN stretching vibration of the amide group at 1420 cm−1. Slight shifts in peaks are due to interactions between PAH and PSS with the acrylamide group. The footprints of PSS are clearly identified in PAAm-PEM as shown in green. Characteristic peaks at 1178 cm^{-1} and 1125 cm^{-1} correspond to the asymmetric stretching vibrations of the S=O; the band at 1037 cm^{-1} (not indicated on the graph) is assigned to the S=O symmetrical stretching vibrations, and the peak at 1008 cm-1 is attributed to aromatic in-plane vibrations [51]. For PSS, peaks at 1037.5, 1009, 1125, and 1178 cm^{-1} are clearly detected. Identification of PAH was rather difficult. Only a peak at 1648 cm-1 could be detected whose intensity increased with increasing number of scans. The peak in figure 8 is obtained after 256

scans. This difficulty might be due to the lower MW of PAH as well as its small amount in the system. The spectra of the pure phospholipid consists of the asymmetric stretch of phosphate at ~1220cm^{-1} and ~1229 cm^{-1}, as well as the symmetric stretch at ~ 1087 cm^{-1}. The C–O–C carboxylic acid ester bond connecting the fatty acids to the glycerol contributes an asymmetric stretch vibration around 1183 cm^{-1} (a broad peak) and the symmetric C–O–C stretch is at 1065 cm-1. In the spectrum shown above, following peaks could be detected: 1178, 1125, 1065 and 1203 cm^{-1}. The observed shifts of the peaks suggest interactions between the lipids and the polyelectrolytes, perhaps between phosphate group of lipid and PAH.

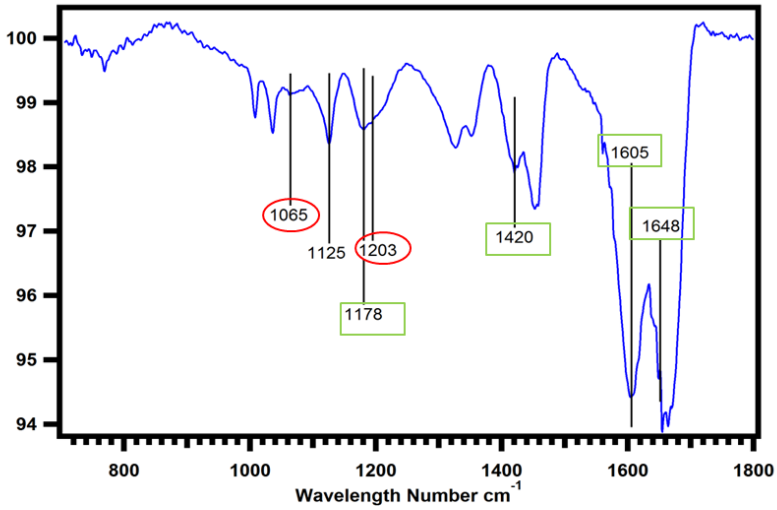

Figure 8: FTIR spectrum of lipid on PAAm-supported PEMs. Characteristic peaks of PAAm gel, PAH, PSS (green) and EggPC are identified (red), confirming adsorption of lipid molecules on PAAm-PEMs.

AFM images were obtained in DI water for the three following systems: lipid bilayer on silica, PAAm- PEMs on silica and lipid bilayer on PAAm- PEMs. All the layers for the samples were assembled in QCM cells and were imaged with in a day after fabrication.

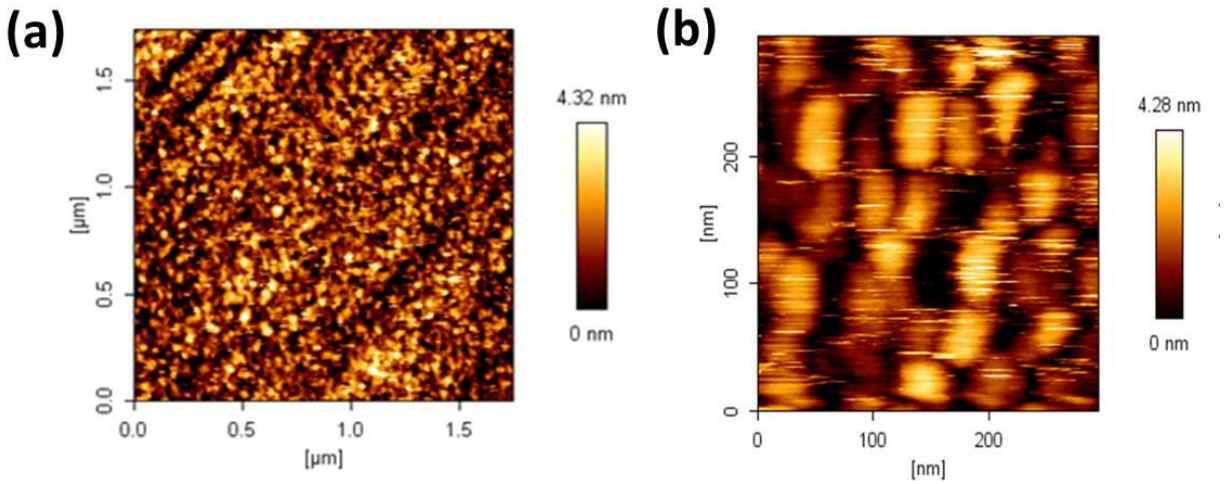

Figure 9: AFM scans obtained via contact mode of a bilayer on silica QCM sensor in water (a) 2 um x 2 um and 9b) 300 nm x 300nm.

Figure 9 (a-b) shows AFM images obtained after formation of bilayer on QCM sensors. The images were obtained in contact mode in water. Since the QCM sensor itself has a similar topography under AFM, the bilayer has closely followed these features. Height scale of both images indicate very small features on the same order of heights as that of a lipid bilayer, having islands (in 300nm x 300nm scan) with width of 42.9 ± 6.6 nm and length of 50.7 ± 15.2 nm. The relative height of 4.28 nm was measured on the images. These results corroborate with the characteristic frequency and dissipation (delta f = -26 Hz and D = 0) changes as seen under QCM-D plots.

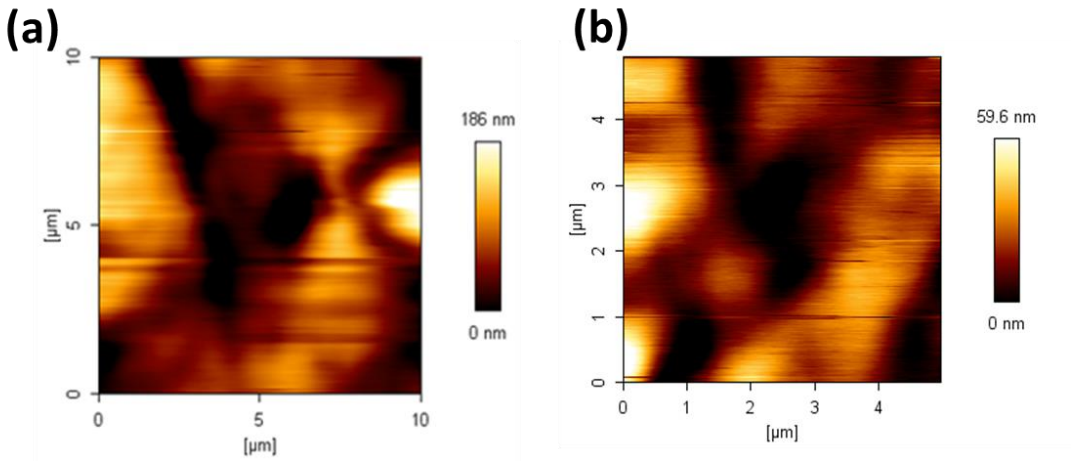

Figure 10 a) & b): AFM images obtained via tapping mode of PAAm-PEMs.

Figure 10 shows AFM images of PAAm-PEM support. PEM layers were assembled layer-by-layer inside the QCM cell and then imaged immediately after. Images were acquired under tapping mode in water, however the images from 10 um x 10 um and 5um x 5 um scan sizes showed features of similar sizes. Such results are probably due to highly swollen nature of hydrogels in water. Further we believe that the grafting of the hydrogels on the gold quartz crystals might not be strong enough and might result in shear of the film, while imaging. To overcome this issue, the samples will be grafted on the glass slide using appropriate linkers and the images will be reproduced in the future. The fact that imaging of these films was difficult shows that the PEMs is supported by a very soft underlying gel.

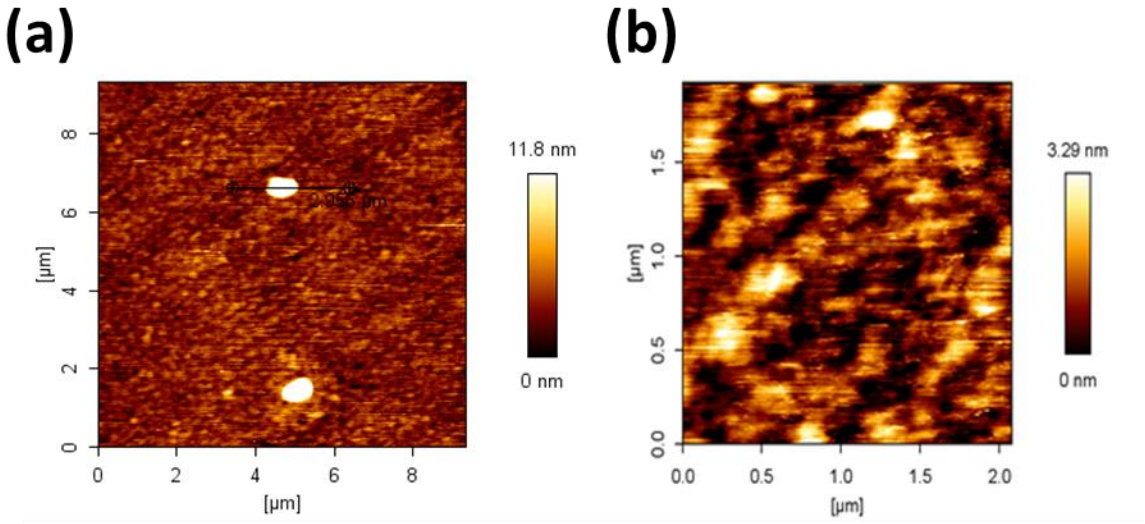

Figure 11: a) AFM image for lipid bilayer on PAAm-PEMs. b) Smaller scan area showing topography details suggesting discontinuous bilayer patches.

Images for lipid bilayers on PAAm-PEM stratified systems were obtained in water with tapping mode. In figure 11a, a 10 um x 10 um image scan shows different surface features in contrast to the ones obtained in Figure 10 (PEM on hydrogel). Figure 11b shows that the bilayer is not continuous and small patches of less than 1 µm are observed. This can be due to the rough and wavy surface of the underlying hydrogels with the PEM layers, which can result in the increase in the heterogeneity of the surface. The formation of PEMs through layer by layer deposition does not result in a uniformly covered surface and there have been studies which suggest formation of islands and their subsequent growth [52]. Since in our system, PEM film has only 5 layers, there is a higher possibility for the formation of islands which haven't coalesced to form a continuous layer. This is also influenced by the initial roughness of the hydrogel surface and its pore size, which will influence the polymer chains to reorient and rearrange during adsorption incurring additional energetic and entropic costs. Hence this results in the formation of bilayer patches. There is also a possibility of areas where PSS was on top (as seen during indentation experiments, see supplementary information) and hence lipid adsorption in these areas will be restricted resulting in the "patchy" surface.

3.2 EFFECT OF MODULUS OF UNDERLYING PAAM ON THE FORMATION OF POLYELECTROLYTE MULTILAYERS

Assembly of PEMs directly on silica surface has been discussed in the previous section. Here the formation of PEM layers on PAAm gels having ~2 kPa and ~8 kPa will be discussed. The hydrogels are porous and thus it is expected that during the layer by layer deposition, the polymers will both absorb and adsorb onto the hydrogel. The PAAm hydrogels are neutral and in the absence of electrostatic forces, the driving force for adsorption are van der Waal's interactions resulting in weak physisorption of the polyelectrolytes.

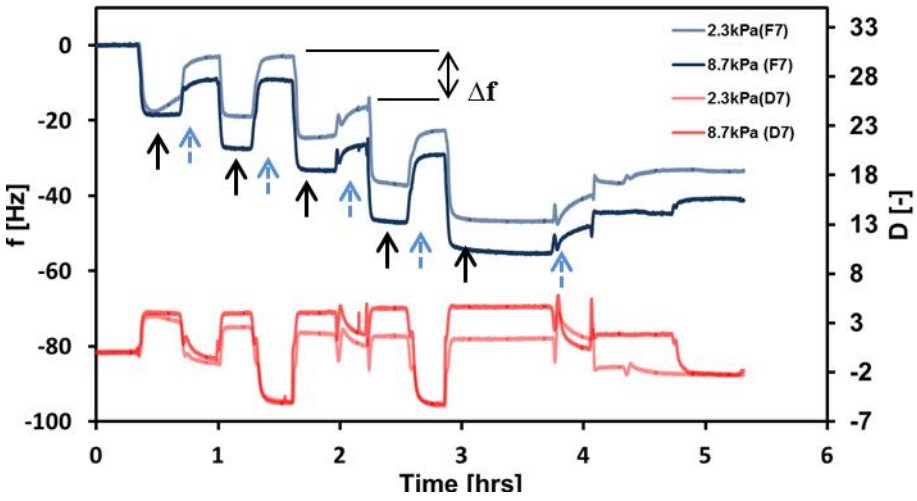

Figure 12: QCM-D plot of PEM formation on ~2 kPa and ~8 kPa PAAm gels. Black arrows indicate PEM injection, Blue arrows show rinsing steps. The PEM architecture is similar on gels of different stiffness suggesting independent behavior of PEM formation.

Figure 12 shows a gradual increase in frequency for both the hydrogels, showing that adsorption, although initially low becomes more significant upon each subsequent step and polymer desorption during rinsing with water is negligible. It is to be noted that if the polymers would only absorb in the pores of the hydrogel (~100 nm in diameter), it is unlikely that sorption (frequency change) would be enhanced in each single step, since the pores would gradually be clogged and the assembly would be self-terminating. Frequency changes can also occur if there is salt going inside pores of hydrogel; hence to be sure, experiments were done to see the frequency changes associated with salt injections (supplementary

information). Therefore, the frequency changes measured here can only correspond to adsorption of polyelectrolytes.

Previous studies have shown that with increase in PAAm modulus, the surface roughness of the hydrogel increases [53]. It can be inferred from this idea that higher adsorption of smaller chain length PAH chains with size ~ 11 nm (from DLS) is expected on rougher surfaces (roughness of hydrogels is larger relative to size of polymer) or stiffer gel since it is more convenient for the shorter polymer chains to conform or adsorb on rougher features in comparison to long chains such as PSS with Rg (radius of gyration) ~ 20 nm (from DLS). This is also seen in Figure 12 where the adsorption of PAH is higher and adsorption of PSS is lower for 8.7 kPa gel in comparison to 2.3 kPa gel.

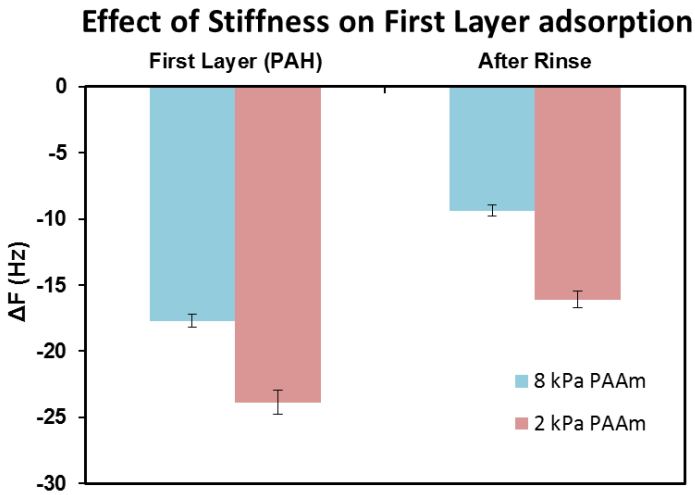

Figure 13: Frequency for the first layer adsorption of PAH on 2.3 kPa and 8.7 kPa gel showing a higher adsorption of PAH on softer gel.

However, a contrast is seen during the first layer deposition as shown in Figure 13. Since the pores for 2.3 kPa gels (red bars) are larger, a greater amount of polymer might penetrate the gel resulting in larger amount of polymer mass adsorption (Δf ~ 25 Hz). Similar trends were observed after rinsing the film. Since 8.7 kPa gel is expected to have pores smaller than those in 2.3 kPa gels [54], a smaller amount of polymer will absorb in the gel, justifying the lower total adsorbed mass (delta f ~ -17 Hz).

Furthermore, the results obtained for the silica-supported PEM film are very similar in magnitude and kinetics as shown in Figure 4. Based on this, and on the AFM images, it can be concluded that the 1st polymer layer (PAH or PSS for the two investigated PEM films) partially penetrates into the hydrogel, whereas the following polymer layers only adsorb at the (macroscopic) hydrogel-liquid interface. This behavior is seen for gels with different pore sizes and moduli. Similar behavior was previously found for

microgel particles [55]. It is, however, not possible to determine the coverage of the hydrogel with the PEM film since the surface area depends on the roughness and the sensitivity of AFM instrument used is insufficient to detect roughness of the hydrogels in a liquid environment.

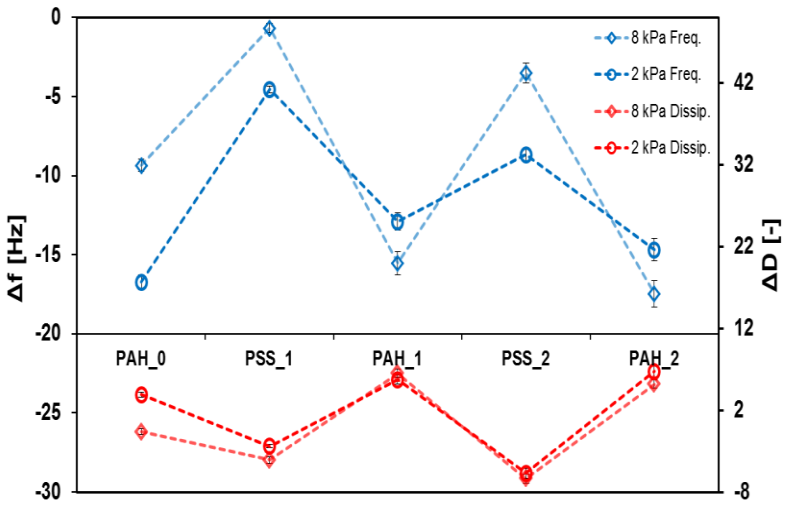

Figure 14: Frequency and dissipation changes of the 7th overtone during PEM formation for each single layer in PAH-(PSS-PAH)$_2$. Values of frequency and dissipation changes were obtained with respect to baseline in water after rinsing the step of each single layer.

Figure 14 shows change in frequency and dissipation during the layer-by-layer deposition of PAH and PSS films on ~8 kpa (diamonds) and ~2 kpa (circles) hydrogels. All values of frequency and dissipation changes have been calculated by considering the previous rinsing step as the baseline as shown in Figure 12. It should also be mentioned here that while the trends for PEM assembly remained the same across experiments, the values slightly differed from experiment to experiment. Hence, conclusions about any minor changes on the PEMs formation due to change in stiffness of the underlying gels were hard to present. However, the results show that the PEMs deposited on these gels have a robust architecture and are highly reproducible. An overall decrease in frequency change and an increase in dissipation change with addition of polyelectrolyte layers suggest adsorption of polyelectrolytes on the hydrogel and a gradual buildup of a layer-by-layer structure. For PSS, the change in frequency and dissipation is always larger than that for PAH. Since PSS has higher chain length and MW, a more negative frequency change due to larger mass is expected. Similarly, a bulky and longer chain of PSS will cause more dissipation compared to shorter chains of PAH. During exposure to PSS solution, the frequency also decreases (negative change); in contrast an overall dissipation decrease ($\Delta D<0$, see figure 12) is seen on hydrogels. This complex change in dissipation is attributed to conformational changes of

PSS up-on adsorption. During polymer adsorption, we expect the polyelectrolyte to adsorb with the conformation in bulk and later to collapse at the surface. A rearrangement of the PSS chains at the surface to optimize electrostatic interactions with the lower PAH layers can lead to a "stiffer" polymer layer that explains the decrease in dissipation. For both hydrogels, however, no significant difference in the PEM architecture or formation is observed.

3.3 FLUORESCENCE RECOVERY AFTER PHOTOBLEACHING (FRAP)

Fig 15a shows a fluorescence image of lipid bilayer deposited on a PAAm gel. The mobility of the lipid layer on the surface of the hydrogel is determined the recovery of fluorescence intensity signal after photo bleaching the highlighted circular region(Fig 15b). Fig 15c shows the normalized fluorescence intensity as a function of time in this region. The graph shows an initial drop in the intensity immediately after photo bleach followed by a fast recovery of fluorescence signal. A subsequent recording of the fluorescence intensity showed that the bleach bilayer did not recover to its original intensity, suggesting an incomplete recovery. Further, the diffusion coefficient for the recovery is estimated as 0.93 $\mu m^2/s$ using the Axelrod method for a circular disc shaped region. Diffusion coefficient for EggPC bilayer on silica surface was reported to be 1.53 $\mu m^2/s$ [56]. Hence**,** the estimated diffusion coefficient values for the lipid layer on PAAm hydrogel is smaller than reported for a bilayer on a bare silica substrate; and this reduced diffusion coefficients on PAAm hydrogel might be the result of the reduced mobility of the lipid molecules due to intermolecular interactions between the lipids and the underlying polyelectrolyte; note that on a silica substrates, the hydrated heads interact less strongly with the underlying surface.

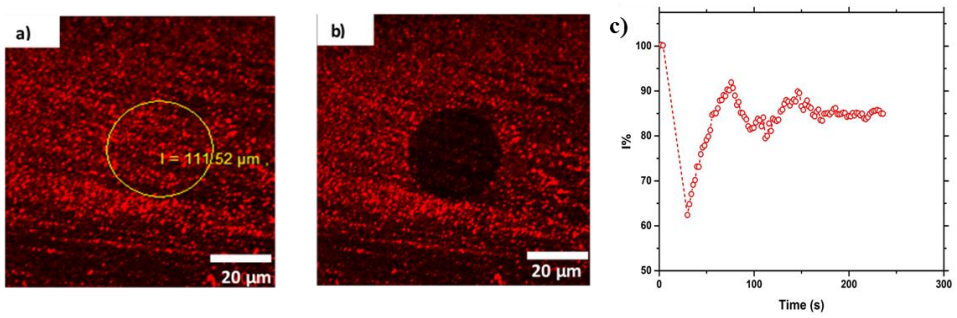

Figure 15. Fluorescence images of a) Lipid bilayer on PAAm-PEM before photo bleaching, (b) recovery of the lipid bilayer after photo bleaching. C) Fluorescence intensity as a function of time after bleaching.

3.4 MECHANICAL CHARACTERIZATION OF THE STRATIFIED SYSTEM

The mechanical properties of the model system and their significance with respect to existing models for cell membranes will be discussed in this section.

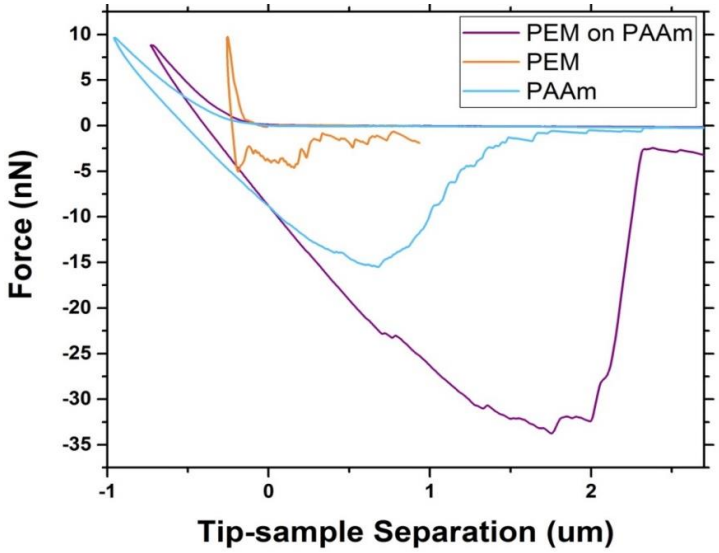

Figure 16: Colloid probe indentation vs. sample separation for three systems: PEM on silica (orange), PAAm on silica (blue) and PAAm supported PEMs (purple). Silica sphere of 10 µm diameter glued to a tipless cantilever of kn = 0.3 N/m was used as a indenter. All curves were obtained in DI water at an approach speed of 5 µm/s and a maximum applied load of 20 nN.

For determining hardness and elasticity of materials, indentation methods have been in practice for a long time. In Figure 16 loading and unloading curves were obtained using AFM on the PAAm hydrogel, PEM on Silica and on PEM-PAAm films. The blue curve shows force vs. depth of indentation (FD) curves for a 2.3 kPa hydrogel, purple corresponds to PAAm-PEM with PAH as the top layer and orange curve represents PEMs on bare silica with PAH as the top layer.

Adhesion interactions between a hydrated polymer and a silica colloid are mainly governed by van der Waals interactions and by electrostatic interactions, when charges are present. For soft polymeric structures such as polymers brushes and hydrogels, the viscoelastic deformation of the film also contributes to the adhesive force. Thus, the adhesion is not only load- dependent but also speed – dependent, i.e. higher loads (contact area) and contact times (low speeds) between the colloid and the polymer film will enhance the interaction energy and will result in higher adhesion forces. As the hydrogels are soft structures, large contact areas are formed between colloid and hydrogel gel resulting in higher adhesion than for less deformable systems, such as PEM on silica, as seen in Figure 16 (blue curve); note that PEM is soft but the film is no thin that there are strong substrate effects. An even higher adhesion during the retraction is obtained for PAAm-PEMs: an electrostatic interaction between the negatively-charged silica sphere and positively-charged amine groups in the PAH top layer will result in an additional attractive force. The electrostatic attraction additionally contributes to adhesion. In contrast, a significantly smaller adhesion is observed for PEMs on bare silica. For PEMs on silica surface, the adhesion was only 16% of that observed for PAAm-PEM. The retraction curve also shows multiple pull-out events indicating ruptures of interaction between the colloid and polymer chains while the AFM probe is retracted. This is due to multiple electrostatic interactions between entangled polymer chains and the colloid; during retraction, polymer chains at the colloid surface are first stretched and by further pulling, the chains are separated from the colloid surface causing multiple ruptures. Similar rupture and pull out events can be seen in the retraction curve for PAAm- PEMs however they are smaller in number due to the lower PEMs adsorbed mass on the hydrogel support compared to the silica substrate.

For characterizing mechanical properties of elastic materials, the Hertz model can be used given that certain conditions are met. To avoid any substrate effects the depth of penetration should be less than 10% of the sample or film height. Furthermore, the contact area radius while indenting should be less than 10% of the radius of curvature of the indenter (R). Hertz model or a planar elastic material in contact with a spherical indenter is given as:

$$F = \frac{4}{3}\frac{E}{1-v^2}R^{0.5}\delta^{1.5}$$

where E is the elastic modulus of the sample , ν is the Poisson's ratio, R is the radius of silica sphere and δ is the indenter displacement.

Figure 17 shows a comparison of the adhesion energy and elastic modulus measured for different systems. Results for the elastic moduli are as predicted and show an increase in modulus with wither increasing crosslinking density of the gel or after deposition of the bilayer. Adhesion energy has been calculated by integrating the area under re-trace of the force curves. It can be seen that softer gels have a higher adhesion since during indentation the material deforms more leading to a higher contact area and hence higher adhesion. Furthermore, having the lipid bilayer on top results in very low adhesion energies, owing to the weaker intermolecular interactions between the colloid and the bilayer; lipids are small molecules compared to polymer chains, and hence, dispersion forces are much smaller. Further, the lipid bilayer increases the elastic modulus (i.e. reduces the contact area), which also contributes to the decrease in adhesion energy. The adhesion energies shown here will be useful in understanding friction measurements discussed in the next section.

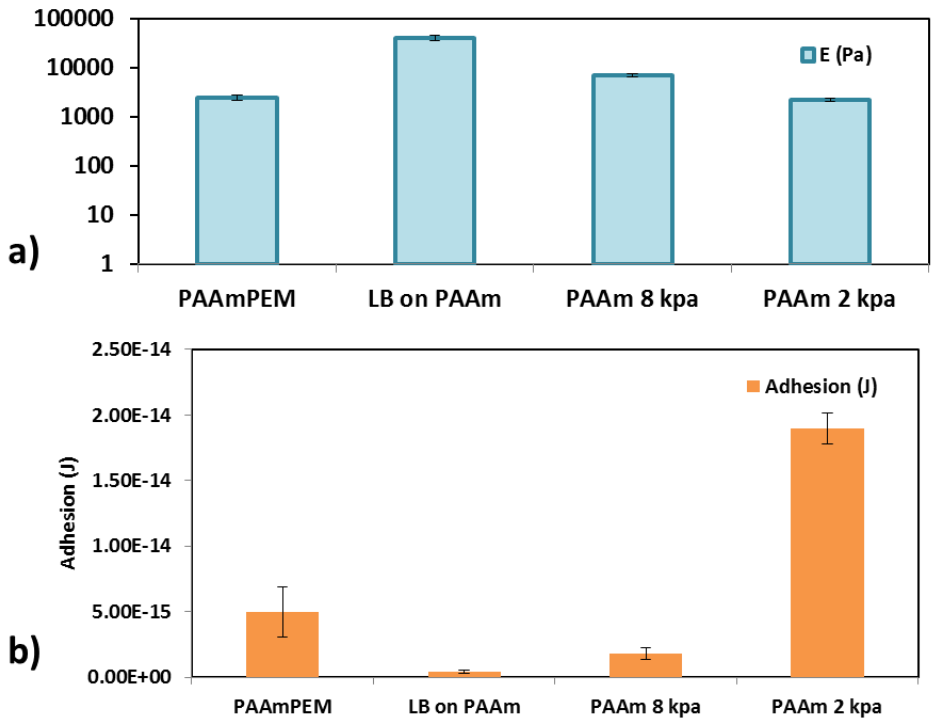

Figure 17: Bar graphs representing a) elastic modulus and b) adhesion energy for PAAm, PAAm-PEMs and LB on PAAm.

In summary, lipid bilayer on softer substrates (PAAm) are a more mechanically relevant model systems to study the NM interactions with cells due to a) negligible substrate effects, b) elastic moduli which are comparable to living cells and c) contact-area dependent interactions. The results here also show that addition of PEMs to the developed system doesn't alter the mechanical properties of underlying support as such.

3.5 NANOMECHANICAL INTERACTIONS OF THE MODEL SYSTEM

AFM sharp tip indentation measurements were carried out with maximum indentation forces of 20 nN and approach speeds of 300 nm/s and 1 μm/s for bilayer on silica and bilayer on PAAm-PEMs, respectively. Different speeds were employed to account for the underlying substrates; for the hydrogel, higher indentation speed facilitates rupture because the gel appears 'stiffer' due to its viscoelastic behavior; on the other hand, lower speeds increase the resolution and facilitate the measure of the bilayer rupturing on silica.

Figure 18a shows the rupture of a lipid bilayer supported on a bare silica substrate. When the AFM probe comes into contact with the lipid bilayer surface, the sharp tip exerts a force on the lipid film and upon reaching a critical value, breaks through the bilayer and hits the hard silica surface. This penetration event is shown as a step in the indentation force curve, after which the AFM probe experiences hard wall repulsion, as expected at a hard contact.

Such bilayer rupture curves have been reported before [57]–[59] and are consistent with the results shown here. The rupture force and the penetration depth are 1.7 ± 0.16 nN and 6.2 ± 0.2 nm, respectively. The penetration depths obtained in our measurements are higher than the film thickness of bilayers [60][61], reasons for which are yet to be investigated.

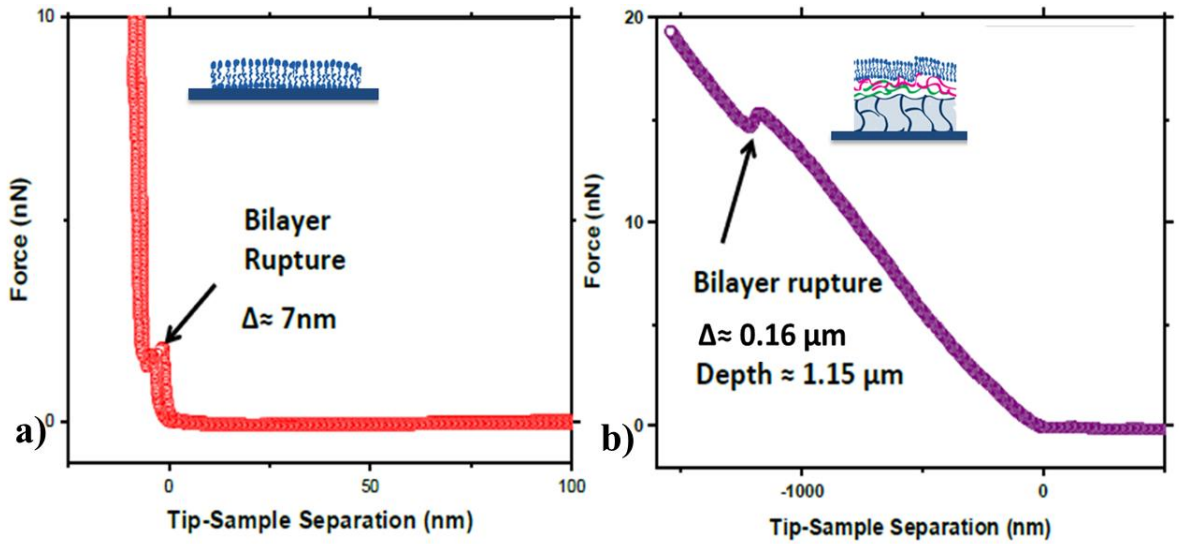

Figure 18: Indentation force vs. sample-separation during bilayer rupture for a) bilayer on silica (red) and for b) bilayer on PAAm-PEMs (purple). Sharp tips having spring constant of 0.3 N/m were used and approach speeds were 300 nm/s and 1 µm/s for bilayer on silica and bilayer on PAAm–PEM support, respectively. Characteristic steps on the force curves indicating bilayer rupture are seen on both systems.

Figure 18b shows the force indentation curves obtained on a bilayer adsorbed on PAAm-PEM films on a QCM gold sensor. The bilayer rupture takes place at much larger indentation depths and indentation forces than those measured on a hard substrate. The reason for this difference is the ability of the hydrogel supported bilayer system to deform under mechanical loading and dissipate energy, as the underlying support provides sufficient compliance for the bilayer to bend. In real cells, the mechanical response consists of response from both the membrane and cell cytoskeleton. However, the elastic forces generated due to the deformation of cytoskeleton during mechanical loading are more dominant than the elastic forces generated by the cell membrane indentation [62]. Here a very similar behavior is shown in the developed model cell membrane system, where due to the underlying gel, the system undergoes a deformation of 1 µm before the membrane rupture occurs. Rupture events were not observed when approach speeds of less than 0.5 µm/s were used. This may be due to the strain-rate dependent (viscoelastic) behavior.

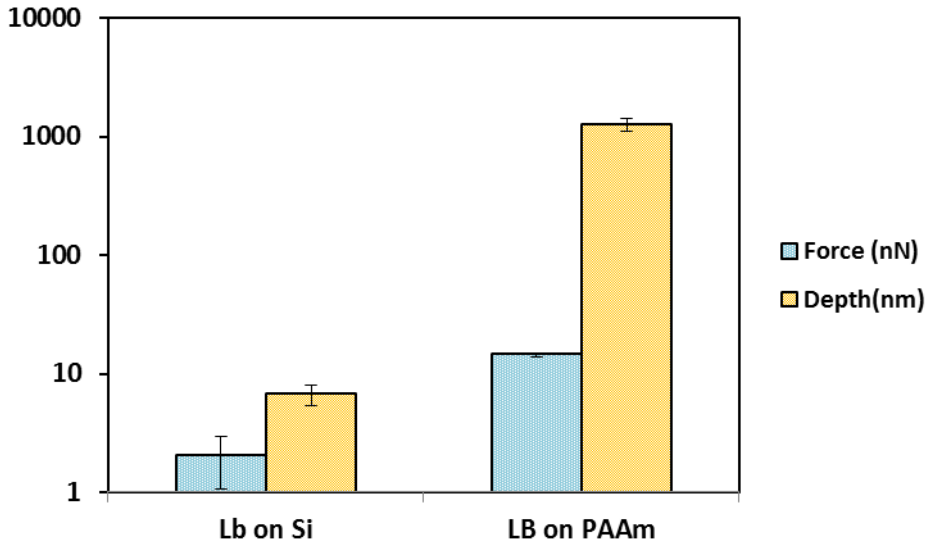

Figure 19: Force and Depth of the ruptures measured for bilayer on silica and bilayer on PAAm-PEMs.

Indentation showed an increase in the penetration depth as well as the rupture force once with the soft support underneath the lipid bilayer, as shown in Fig 19. Rupture force and penetration depth for bilayer on silica were measured to be 2.01 ± 0.94 nN and 6.69 ± 1.34 nm respectively while for bilayer on PAAm-PEM were 14.47 ± 0.51 nN and 1.26 ± 0.15 µm respectively. This shows that the developed model system undergoes considerable deformation before and after the rupture, which is similar to the behavior of a real cell membrane in which the cytoskeleton deforms upon an applied force.

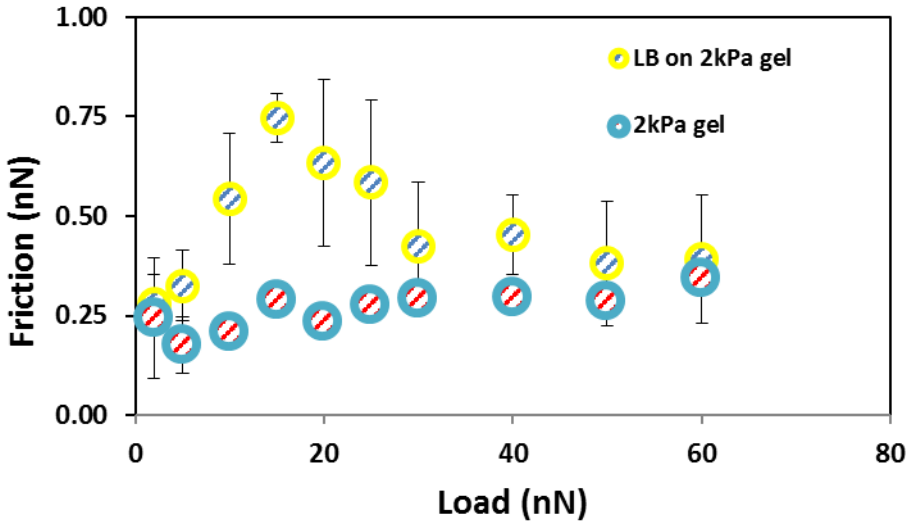

Figure 20: Friction vs Load for lipid bilayer on a 2kPa hydrogel, and for the hydrogel. Measurements were done with a sintered silica tip (radius=80 nm, tip speed= 1µm/s).

Figure 20 summarizes friction forces as a function of load for PAAm hydrogel (E ~ 2 kPa) and LB on PAAm hydrogel using a blunt silica tip (radius ≈ 80nm) at a sliding speed of 1µm/s. Friction forces show a continuous increase with normal load for PAAm hydrogels. While the friction measurements for bilayer on PAAm hydrogel initially show a more pronounced increase in friction force with applied load than the hydrogel, it was followed by a transition at ~ 15 - 30 nN, where a decrease in friction force with load is observed. Finally, at higher loads (i.e. > 40 nN), the friction force increase with load on hydrogel and LB layer on hydrogel are similar. Friction coefficients –defined as the ratio between friction force and normal load- after the transition- are obtained to be 0.002, similar to that obtained on hydrogels.

The friction loops on hydrogel are tilted unlike to those observed in ref.[63] and the tilt is shown to increase with increase in the applied normal load (Fig. 21a). The blunt AFM tip (r=80 nm) penetrates into the hydrogel upon contact and with increase in normal load (i.e. contact area), the interactions between the tip and hydrogel increase, thereby leading to higher friction forces. Further, as the tip indents deeper into the hydrogel, the shearing of the tip through the highly hydrated hydrogel network increases the lateral tilting of the cantilever (friction loop tilt) and only at high stroke lengths steady state sliding can be observed (not observed in Fig. 21a). The friction loops obtained on PAAm-supported bilayers show similar tilt as those observed for PAAm hydrogel (Figs. 21 b & c) at similar applied loads. However, the friction loop for LB on hydrogel shows discontinuities and multiple ruptures, especially at

low loads (Fig. 21 b). This discontinuities can have various explanations: they can result from either multiple ruptures of the bilayer or/and ruptures of the interactions between the tip and the PEM layer (with an excess positive charge), since as mentioned before, the lipid bilayer forms discontinuous patches. After the transition (30nN) friction loops for full system are smooth and are very similar to those observed on hydrogel (Fig. 21 c). This suggests the possibility of bilayer removal from the surface after the transition load. A decrease in hydration of the lipid heads is unlikely, since friction should increase under these conditions. Speed-dependent friction force measurements will be performed to provide some insight into the change of the friction mechanism.

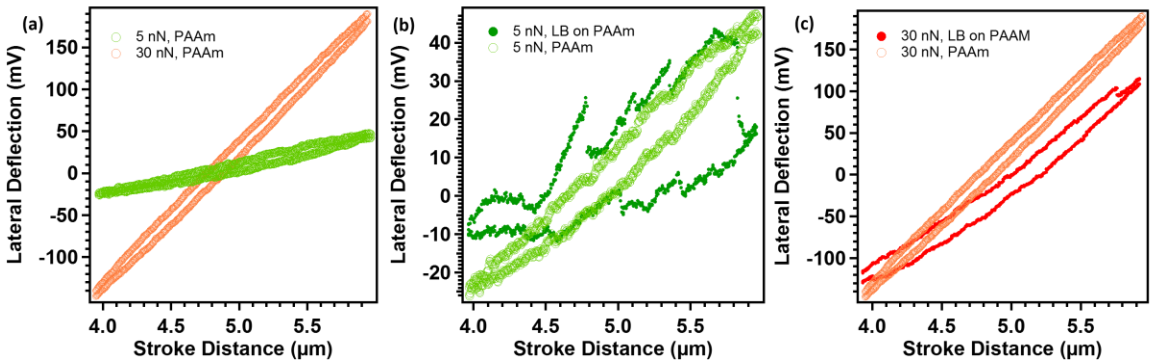

Figure 21: (a) Friction loops (lateral Deflection vs stroke distance) for PAAm hydrogel at 5 nN and 10 nN. Comparison of friction loops obtained on lipid bilayer on PAAm and PAAm hydrogel at (b) 5 nN and (c) 30 nN.

In order to further indicate that the observed transition for lipids on PAAm hydrogels are caused by the rupture process but not from surface interactions, we measured the friction forces as function of load using a gold AFM tip (Fig. 21). Furthermore, since the gold-based nanomaterials are highly employed in cancer therapeutics due to their interesting electronic and optical properties, measuring interaction forces between the gold sharp tips and cell membrane is interesting.

Unlike silica probes, the gold AFM tips are positively charged in aqueous media [64] which is expected to vary surface interactions, e.g. the interactions between the PEM and the tip. Further, the Au AFM tips are sharper (radius ~ 25 nm, as received) in comparison to the blunt silica probes (~ radius ~ 80 nm, obtained by thermal annealing) used in the previous section. Fig 22 summarizes the friction forces as a function of applied load on 2 kPa PAAm hydrogel and lipid bilayer on PAAm hydrogel using the Au AFM tip.

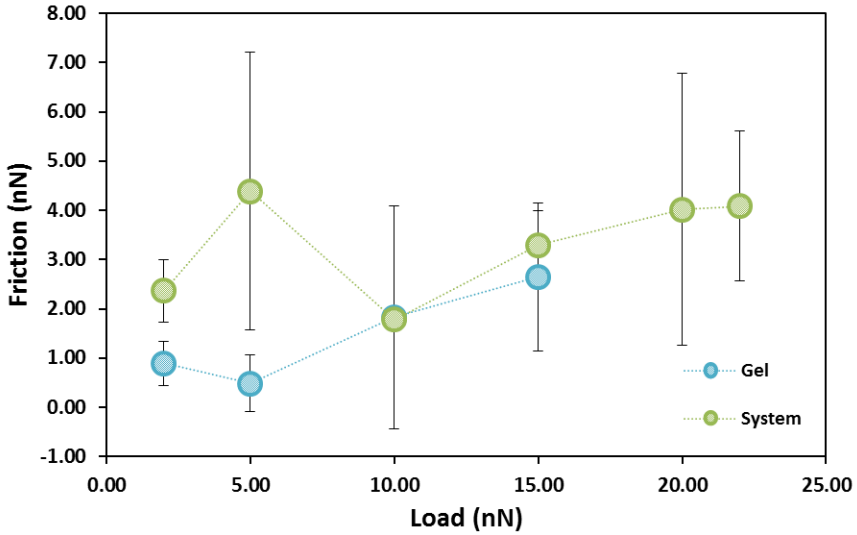

Figure 22: Friction force vs load plots for PAAm (blue) and bilayer on PAAm systems (green) obtained with a Au tip. The characteristic transition for bilayer on PAAm system is observed at ~ 5 nN.

The transition on friction vs. normal load for bilayer on PAAm using Au tip shows conformity with the results obtained using a blunt silica probe (Fig. 20), where beyond a transition load (~ 5 nN) a sudden decrease in friction force is observed. Beyond a normal load of 10 nN, the friction forces as a function of load on the two systems are similar. The observed similar transitions in lipid on PAAm system in spite of change in surface chemistry of the tip clearly indicate the effect of an underlying physical mechanism; since the interactions between the PAH upper layer and the Au tip are (electrostatically) repulsive, it is more likely that the transition results from the rupture of the bilayer on the hydrogel at high contact pressure (P~30kPa). However, the transition loads obtained using Au tips were smaller than those obtained using the silica probes (~ 15-20 nN, Fig. 20). For Au probes, the tip radius is smaller than sintered silica tips resulting in higher contact pressures at similar applied loads. If the observed transition indicates physical rupturing of the bilayer, then the transition will happen at lower forces with decrease in tip size, which is in agreement with our results.

However, silica and gold tips have different surface chemistries, which will play a role in measured friction forces. Higher friction forces were observed for the bilayer on the PAAm hydrogel using Au tip in comparison to silica tip. Unlike Au tip, silica tips form a strong hydration layer in aqueous

medium, which can reduce the surface interactions between the probe and the hydrated lipid or polymer chains; further, an electrostatic attraction between the Au tips and the weakly negatively charged lipid heads is also possible. The difference in interaction forces can be observed in Fig 23, where the indentation force-distance curve with Au tip shows large adhesion in comparison to the silica tip, suggesting higher interaction forces result in higher friction forces between Au tip and full system.

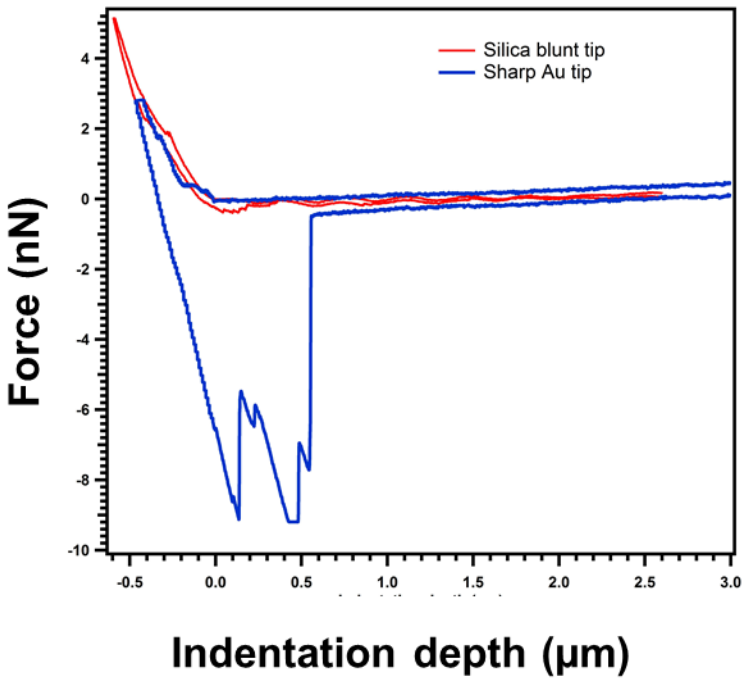

Figure 23: Force vs Indentation plots of lipid bilayer on hydrogel with Au (blue) and silica (red) AFM tips.

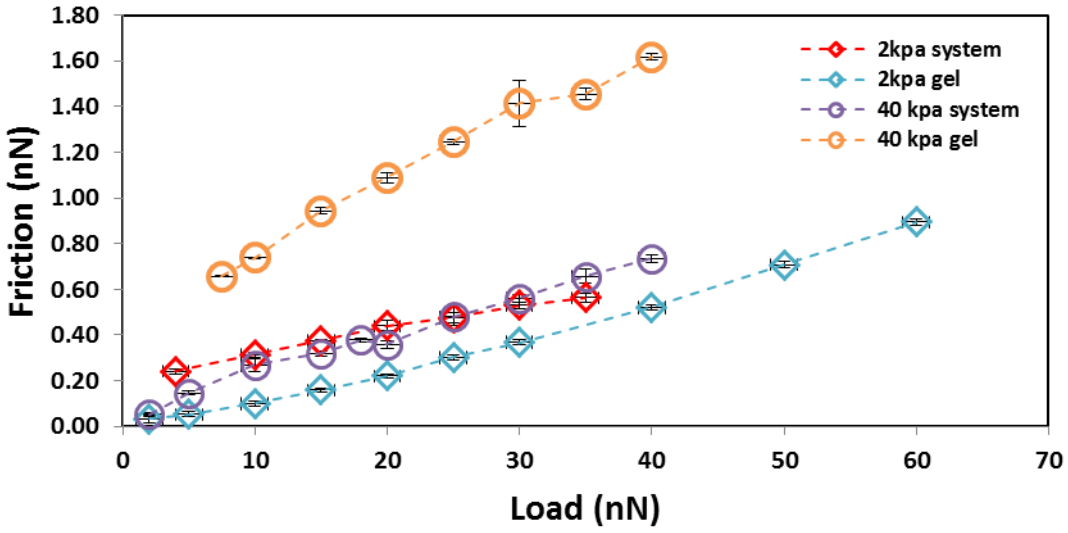

Figure 24: Friction vs load for different systems measured by colloid probe lateral force microscopy. Systems: red: bilayer on 2kPa PAAm; blue: 2kPa PAAm; purple: bilayer on 40kPa PAAm; orange: 40kPa PAAm

The results for the friction force vs. load performed using a silica colloid (r = 5µm) are shown in Fig 24. The friction forces for 2 kPa PAAm gel are smaller than those for the hydrogel-supported bilayer. In contrast, the 40 kPa PAAm gel shows higher friction forces in comparison to the hydrogel (40 kPa)supported bilayer. Higher hydration for 2 kPa PAAm gel, in comparison to 40 kPa hydrogel, allows the fluid to support the normal load at the interface and reduces the interactions between polyacrylamide chains and silica probe. This results in smaller friction forces for 2 kPa PAAm hydrogel in comparison to the more crosslinked hydrogel (40 kPa). The addition of lipid bilayer on 2 kPa PAAm hydrogel might locally stiffen the interface and increase the surface roughness increasing contact area and the friction force; in contrast, lipid bilayer deposited on the 40kPa hydrogel is shown to be a more lubricating surface than the hydrogel; the origin for this reduction is not clear yet but might be related to a reduction in interfacial interactions and adhesion energy. This is currently under investigation. The characteristic transition shown in blunt-tip friction measurements, is not seen here, which is, as discussed before, due to larger contact areas and lower contact pressures achieved with the colloid.

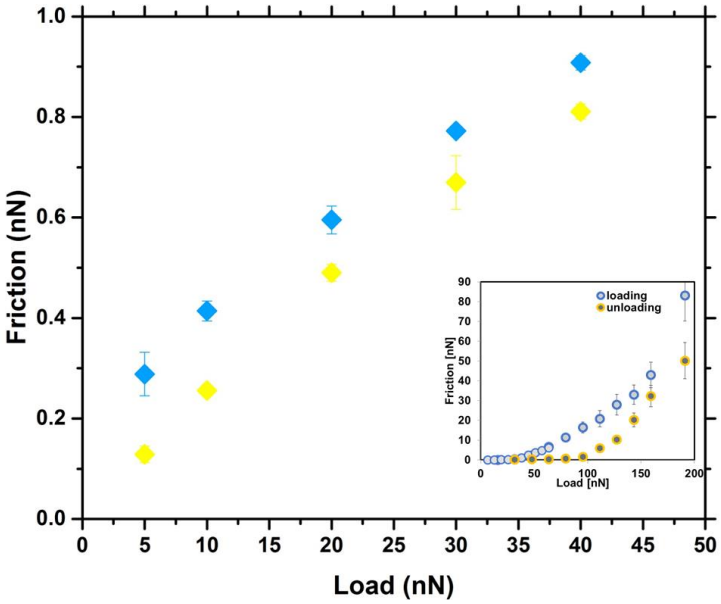

Figure 25: Friction vs. load during load increase (blue) and decrease (yellow) for bilayer deposited on a hydrogel, measured by colloid probe lateral force microscopy. The inset shows similar results for the bilayer on bare silica.

Self-healing of lipid bilayers has been previously reported and also confirmed in our experiments (Fig 25 inset) [65]. It was shown that with progressive sliding, the friction of the bilayer reaches lower values, indicating that the lipid molecules organize themselves to form more ordered layers. The reversibility of the frictional behavior as well as the decrease in friction was tested by measuring friction forces during load increase and decrease along the same scan line. A similar trend is shown in Fig 25 for the lipid bilayer on PAAm, in which the friction force during load decreases and it results in lower friction force, suggesting that maybe the bilayer is becoming more ordered due to repeated sliding of the tip at the interface.

These results not only give some insights into the mechanical behavior of the developed system but also provide some very interesting tribological results. Friction measurements here show that having a bilayer on top of stiffer gels can lead to lower friction values. Furthermore, the bilayer on hydrogels provides robust frictional properties and in fact, it can self-heal. These are preliminary tribological results, which could be further explored for understanding cartilage and ocular lubrication. Additionally, these results might open new opportunities in development of devices or implants such as catheters or ocular lenses where biocompatiblity and effective lubrication is essential.

CHAPTER 4
CONCLUSIONS

Successful development of a physiologically relevant non-living model system for cell membranes with tunable mechanical properties has been shown. QCM results show successful single step formation of lipid bilayer on top of PAAm gels having modulus in the range of 2-4 kPa with a PEM as linker between the lipid membrane and the hydrogel. Presence of PAH as the top layer increased electrostatic interactions between the lipid vesicles and support surface, leading to immediate rupturing of vesicles and bilayer formation. Frequency change of -30 Hz indicates only an increase in the surface area for adsorption compared to the frequency shift upon self-assembly of the lipid bilayer on silica, which is due to a higher roughness of PAAm-PEM surface. Furthermore, a dissipation value of 0.8×10^{-6} confirms presence of a rigid film on the surface.

PEMs architecture was thoroughly characterized by varying underlying gel stiffness and porosity and increasing the number of deposited layers and it was shown that the layer-by-layer structure was independent of these two factors. It was also confirmed that no significant deposition of polymers inside the hydrogels was taking place. Voigt's model fitting showed the thickness of PEMs layer to be around 12 nm.

AFM images of bilayer on hard substrates, PAAm with PEMs on top and lipid bilayer on PAAm supported PEMs were compared and it was shown that bilayer patches formed on PAAm supported PEMs which made surface of the hydrogels more rigid and easier to image by AFM. Smaller scan areas show height profiles on the order of a silica-supported lipid bilayer thickness suggesting the AFM tip passes over a bilayer patch and hits bare silica surface underneath. Lipid bilayers with soft underlying supports were compared to bilayers having a hard substrate via

colloid probe indentation, which showed that modulus and adhesion forces differed by factors of 40 and 7, respectively. Furthermore, bilayer rupture forces increased from ~2 nN to ~15 nN for bilayer on silica and bilayer on PAAm-PEMs and the penetration depth increased from ~ 6nm to ~1.5μm. Hence the deformation behavior of the developed model system mimics that of real cell behavior, where the cell matrix deforms upon exposure to external stresses. Friction experiments revealed a reproducible transition region corresponding to the rupture of the lipid bilayer at higher forces. Colloid tip interactions also revealed lubrication limitation of the proposed system and showed that the friction can be maintained after cyclic loading and unloading of the system. The frictional properties of this model system can be further studied and developed for understanding mechanisms behind cartilage and ocular lubrication and can also help in designing biomaterials and implants.

REFERENCES

[1] C. W. Yong, “Study of interactions between polymer nanoparticles and cell membranes at atomistic levels,” 2014.

[2] M. a. Browne, A. Dissanayake, T. S. Galloway, D. M. Lowe, and R. C. Thompson, “Ingested microscopic plastic translocates to the circulatory system of the mussel, Mytilus edulis (L.),” *Environ. Sci. Technol.*, vol. 42, no. 13, pp. 5026–5031, 2008.

[3] S. Morandat, S. Azouzi, E. Beauvais, A. Mastouri, and K. El Kirat, “Atomic force microscopy of model lipid membranes.,” *Anal. Bioanal. Chem.*, vol. 405, no. 5, pp. 1445–61, 2013.

[4] A. E. Nel, L. Mädler, D. Velegol, T. Xia, E. M. V Hoek, P. Somasundaran, F. Klaessig, V. Castranova, and M. Thompson, “Understanding biophysicochemical interactions at the nano-bio interface.,” *Nat. Mater.*, vol. 8, no. 7, pp. 543–557, 2009.

[5] J. Raedler, H. Strey, and E. Sackmann, “Phenomenology and Kinetics of Lipid Bilayer Spreading on Hydrophilic Surfaces,” *Langmuir*, vol. 11, no. 11, pp. 4539–4548, 1995.

[6] W. Knoll, “Polyelectrolyte-supported lipid membranes,” vol. 56, pp. 175–178, 2002.

[7] I. Reviakine and A. Brisson, “Formation of Supported Phospholipid Bilayers from Unilamellar Vesicles Investigated by Atomic Force Microscopy,” no. 16, pp. 1806–1815, 2000.

[8] N. Hain, M. Gallego, and I. Reviakine, “Unraveling supported lipid bilayer formation kinetics: Osmotic effects,” *Langmuir*, vol. 29, no. 7, pp. 2282–2288, 2013.

[9] P. S. Cremer and S. G. Boxer, “Formation and Spreading of Lipid Bilayers on Planar Glass Supports,” vol. 291, pp. 2554–2559, 1999.

[10] C. Hamai, P. S. Cremer, and S. M. Musser, “Single giant vesicle rupture events reveal multiple mechanisms of glass-supported bilayer formation.,” *Biophys. J.*, vol. 92, no. 6, pp. 1988–1999, 2007.

[11] M. Schulz, A. Olubummo, and W. H. Binder, “Beyond the lipid-bilayer: interaction of polymers and nanoparticles with membranes,” *Soft Matter*, vol. 8, no. 18, p. 4849, 2012.

[12] X. Lin, C. Wang, M. Wang, K. Fang, and N. Gu, “Computer Simulation of the Effects of Nanoparticles’ Adsorption on the Properties of Supported Lipid Bilayer,” *J. Phys. Chem.*, vol. 116, pp. 17960–17968, 2012.

[13] B. L. and G. P., “Influence of the fluidity of the membrane on the response of microorganisms to environmental stresses,” *Appl. Microbiol. Biotechnol.*, vol. 57, no. 1–2, pp. 34–42, 2001.

[14] A. M. Schrader, S. H. Donaldson, J. Song, C.-Y. Cheng, D. W. Lee, S. Han, and J. N. Israelachvili, “Correlating steric hydration forces with water dynamics through surface force and diffusion NMR measurements in a lipid–DMSO–H $_2$ O system,” *Proc. Natl. Acad. Sci.*, vol. 112, no. 34, p. 201512325, 2015.

[15] N.-J. Cho, J. a Jackman, M. Liu, and C. W. Frank, “pH-driven assembly of various supported lipid platforms: a comparative study on silicon oxide and titanium oxide.,” *Langmuir*, vol. 27, no. 7, pp. 3739–48, 2011.

[16] T. H. Anderson, Y. Min, K. L. Weirich, H. Zeng, D. Fygenson, and J. N. Israelachvili, “Formation of Supported Bilayers on Silica Substrates,” *Langmuir*, vol. 25, no. 12, pp. 6997–7005, 2009.

[17] L. Tamm and H. McConnell, “Supported phospholipid bilayers,” *Biophys. J.*, vol. 47, no. 1, pp. 105–113, 1985.

[18] A. O. Hohner, M. P. C. David, and J. O. Rädler, “Controlled solvent-exchange deposition of phospholipid membranes onto solid surfaces.,” *Biointerphases*, vol. 5, no. 1, pp. 1–8, 2010.

[19] F. Tiberg, I. Harwigsson, and M. Malmsten, “Formation of model lipid bilayers at the silica-water interface by co-adsorption with non-ionic dodecyl maltoside surfactant.,” *Eur. Biophys. J.*, vol. 29, pp. 196–203, 2000.

[20] M. D. Mager and N. a. Melosh, “Lipid bilayer deposition and patterning via air bubble collapse,” *Langmuir*, vol. 23, no. 18, pp. 9369–9377, 2007.

[21] S.-Y. Jung, M. A. Holden, P. S. Cremer, and C. P. Collier, “Two-Component Membrane Lithography via Lipid Backfilling,” *ChemPhysChem*, vol. 6, no. 3, pp. 423–426, 2005.

[22] G. J. Hardy, R. Nayak, and S. Zauscher, “Model cell membranes: Techniques to form complex biomimetic supported lipid bilayers via vesicle fusion.,” *Curr. Opin. Colloid Interface Sci.*, vol. 18, no. 5, pp. 448–458, 2013.

[23] E. Reimhult, F. Höök, and B. Kasemo, “Intact vesicle adsorption and supported biomembrane formation from vesicles in solution: Influence of surface chemistry, vesicle size, temperature, and osmotic pressure,” *Langmuir*, vol. 19, no. 5, pp. 1681–1691, 2003.

[24] R. Tero, “Substrate Effects on the Formation Process, Structure and Physicochemical Properties of Supported Lipid Bilayers,” *Materials (Basel).*, vol. 5, no. 12, pp. 2658–2680, 2012.

[25] M. Sundh, S. Svedhem, and D. S. Sutherland, “Influence of phase separating lipids on supported lipid bilayer formation at SiO2 surfaces.,” *Phys. Chem. Chem. Phys.*, vol. 12, no. 2, pp. 453–460, 2010.

[26] R. Merkel, E. Sackmann, and E. Evans, “Molecular friction and epitactic coupling between monolayers in supported bilayers,” *J. Phys.*, vol. 50, no. 12, pp. 1535–1555, 1989.

[27] A. Brian and H. McConnell, “Allogeneic stimulation of cytotoxic T cells by supported planar

membranes," *Proc. Natl. …*, vol. 81, no. October, pp. 6159–6163, 1984.

[28] H. M. McConnell, T. H. Watts, R. M. Weis, and a a Brian, "Supported planar membranes in studies of cell-cell recognition in the immune system.," *Biochim. Biophys. Acta*, vol. 864, pp. 95–106, 1986.

[29] M. Puig-de-morales-marinkovic, K. T. Turner, J. P. Butler, J. J. Fredberg, S. Suresh, T. Kt, B. Jp, and S. S. Viscoelasticity, "Viscoelasticity of the human red blood cell," *Am. J. Physiol. Physiol.*, vol. 293, pp. C597–C605, 2007.

[30] C. a. Naumann, O. Prucker, T. Lehmann, J. Rühe, W. Knoll, and C. W. Frank, "The polymer-supported phospholipid bilayer: Tethering as a new approach to substrate-membrane stabilization," *Biomacromolecules*, vol. 3, no. 1, pp. 27–35, 2002.

[31] J. Schmitt, B. Danner, and T. M. Bayerl, "Polymer cushions in supported phospholipid bilayers reduce significantly the frictional drag between bilayer and solid surface," *Langmuir*, vol. 17, no. 1, pp. 244–246, 2001.

[32] T. Cassier, A. Sinner, A. Offenhäuser, and H. Möhwald, "Homogeneity, electrical resistivity and lateral diffusion of lipid bilayers coupled to polyelectrolyte multilayers," *Colloids Surfaces B Biointerfaces*, vol. 15, pp. 215–225, 1999.

[33] O. M. Tanchak, K. G. Yager, H. Fritzsche, T. Harroun, J. Katsaras, and C. J. Barrett, "Water distribution in multilayers of weak polyelectrolytes," *Langmuir*, vol. 22, no. 11, pp. 5137–5143, 2006.

[34] E. Sackmann, "Supported membranes: scientific and practical applications.," *Science*, vol. 271, no. 5245, pp. 43–48, 1996.

[35] M. Tanaka and E. Sackmann, "Polymer-supported membranes as models of the cell surface.," *Nature*, vol. 437, no. 7059, pp. 656–663, 2005.

[36] P. F. Kiser, G. Wilson, and D. Needham, "Lipid-coated microgels for the triggered release of doxorubicin," *J. Control. Release*, vol. 68, no. 1, pp. 9–22, 2000.

[37] B. G. De Geest, B. G. Stubbe, A. M. Jonas, T. Van Thienen, W. L. J. Hinrichs, J. Demeester, and S. C. De Smedt, "Self-exploding lipid-coated microgels," *Biomacromolecules*, vol. 7, no. 1, pp. 373–379, 2006.

[38] K. Simons and W. L. C. Vaz, "Model Systems, Lipid Rafts, and Cell Membranes [1]," *Annu. Rev. Biophys. Biomol. Struct.*, vol. 33, no. 1, pp. 269–295, 2004.

[39] R. V. Goreham, V. C. Thompson, Y. Samura, C. T. Gibson, J. G. Shapter, and I. Köper, "Interaction of Silver Nanoparticles with Tethered Bilayer Lipid Membranes," *Langmuir*, vol. 31, no. 21, pp. 5868–5874, 2015.

[40] E. Reimhult, M. Zäch, F. Höök, and B. Kasemo, "A multitechnique study of liposome adsorption

on Au and lipid bilayer formation on SiO2," *Langmuir*, vol. 22, no. 9, pp. 3313–3319, 2006.

[41] J. R. Tse and A. J. Engler, "Preparation of hydrogel substrates with tunable mechanical properties," *Curr. Protoc. Cell Biol.*, no. SUPPL. 47, pp. 1–16, 2010.

[42] C. A. Keller and B. Kasemo, "Surface specific kinetics of lipid vesicle adsorption measured with a quartz crystal microbalance," *Biophys. J.*, vol. 75, no. 3, pp. 1397–1402, 1998.

[43] R. P. Richter, R. Bérat, and A. R. Brisson, "Formation of solid-supported lipid bilayers: an integrated view.," *Langmuir*, vol. 22, no. 8, pp. 3497–505, 2006.

[44] Y. Shin, W. H. Cheung, T. T. M. Ho, K. E. Bremmell, and D. A. Beattie, "Insights into hydrophobic molecule release from polyelectrolyte multilayer films using in situ and ex situ techniques," *Phys. Chem. Chem. Phys.*, vol. 16, no. 40, pp. 22409–22417, 2014.

[45] E. Reimhult, M. Zäch, F. Höök, and B. Kasemo, "A multitechnique study of liposome adsorption on Au and lipid bilayer formation on SiO2," *Langmuir*, vol. 22, no. 9, pp. 3313–3319, 2006.

[46] M. Schönhoff, "Layered polyelectrolyte complexes: physics of formation and molecular properties," *J. Phys. Condens. Matter*, vol. 15, no. 49, pp. R1781–R1808, 2003.

[47] M. Fischlechner, M. Zaulig, S. Meyer, I. Estrela-Lopis, L. Cuéllar, J. Irigoyen, P. Pescador, M. Brumen, P. Messner, S. Moya, and E. Donath, "Lipid layers on polyelectrolyte multilayer supports," *Soft Matter*, vol. 4, pp. 2245–2258, 2008.

[48] G. J. Hardy, R. Nayak, and S. Zauscher, "Model cell membranes: Techniques to form complex biomimetic supported lipid bilayers via vesicle fusion.," *Curr. Opin. colloid {&} interface Sci.*, vol. 18, no. 5, pp. 448–458, 2013.

[49] N.-J. Cho, J. a Jackman, M. Liu, and C. W. Frank, "pH-driven assembly of various supported lipid platforms: a comparative study on silicon oxide and titanium oxide.," *Langmuir*, vol. 27, no. 7, pp. 3739–3748, 2011.

[50] P. C. Nalam, L. Daikhin, R. M. Espinosa-Marzal, J. Clasohm, M. Urbakh, and N. D. Spencer, "Two-Fluid Model for the Interpretation of Quartz Crystal Microbalance Response: Tuning Properties of Polymer Brushes with Solvent Mixtures," *J. Phys. Chem. C*, vol. 117, pp. 4533–4543, 2013.

[51] L. T. Chiem, L. Huynh, J. Ralston, and D. A. Beattie, "An in situ ATR-FTIR study of polyacrylamide adsorption at the talc surface," *J. Colloid Interface Sci.*, vol. 297, no. 1, pp. 54–61, 2006.

[52] D. Volodkin and R. Von Klitzing, "Competing mechanisms in polyelectrolyte multilayer formation and swelling: Polycation-polyanion pairing vs. polyelectrolyte-ion pairing," *Curr. Opin. Colloid Interface Sci.*, vol. 19, no. 1, pp. 25–31, 2014.

[53] A. Li, E. M. Benetti, D. Tranchida, J. N. Clasohm, H. Schönherr, and N. D. Spencer, "Surface-

grafted, covalently cross-linked hydrogel brushes with tunable interfacial and bulk properties," *Macromolecules*, vol. 44, no. 13, pp. 5344–5351, 2011.

[54] D. L. Holmes and N. C. Stellwagen, "Estimation of polyacrylamide gel pore size from Ferguson plots of linear DNA fragments. II. Comparison of gels with different crosslinker concentrations, added agarose and added linear polyacrylamide.," *Electrophoresis*, vol. 12, no. 9, pp. 612–619, 1991.

[55] B. G. De Geest, C. D??jugnat, E. Verhoeven, G. B. Sukhorukov, A. M. Jonas, J. Plain, J. Demeester, and S. C. De Smedt, "Layer-by-layer coating of degradable microgels for pulsed drug delivery," *J. Control. Release*, vol. 116, no. 2 SPEC. ISS., pp. 159–169, 2006.

[56] Y. K. Lee, S. Kim, J.-W. Oh, and J.-M. Nam, "Massively parallel and highly quantitative single-particle analysis on interactions between nanoparticles on supported lipid bilayer.," *J. Am. Chem. Soc.*, vol. 136, no. 10, pp. 4081–8, 2014.

[57] Z. Leonenko, E. Finot, and D. Cramb, "AFM study of interaction forces in supported planar DPPC bilayers in the presence of general anesthetic halothane," *Biochim. Biophys. Acta - Biomembr.*, vol. 1758, no. 4, pp. 487–492, 2006.

[58] S. Morandat, S. Azouzi, E. Beauvais, A. Mastouri, and K. El Kirat, "Atomic force microscopy of model lipid membranes.," *Anal. Bioanal. Chem.*, vol. 405, no. 5, pp. 1445–1461, 2013.

[59] J. Schneider, Y. F. Dufrene, W. R. Barger, and G. U. Lee, "Atomic force microscope image contrast mechanisms on supported lipid bilayers.," *Biophys J*, vol. 79, no. 2, pp. 1107–1118, 2000.

[60] H. Schönherr, J. M. Johnson, P. Lenz, C. W. Frank, and S. G. Boxer, "Vesicle adsorption and lipid bilayer formation on glass studied by atomic force microscopy," *Langmuir*, vol. 20, no. 26, pp. 11600–11606, 2004.

[61] X. Liang, G. Mao, and K. Y. S. Ng, "Probing small unilamellar EggPC vesicles on mica surface by atomic force microscopy," *Colloids Surfaces B Biointerfaces*, vol. 34, no. 1, pp. 41–51, 2004.

[62] L. Sirghi, U. Alexandru, and I. Cuza, "Atomic Force Microscopy indentation of living cells," no. November, pp. 433–440, 2015.

[63] A. C. Dunn, W. G. Sawyer, and T. E. Angelini, "Gemini Interfaces in Aqueous Lubrication with Hydrogels," pp. 59–66, 2014.

[64] R. Tivony and J. Klein, "Probing the Surface Properties of Gold at Low Electrolyte Concentration," 2016.

[65] R. Sorkin, N. Kampf, L. Zhu, and J. Klein, "Hydration lubrication and shear-induced self-healing of lipid bilayer boundary lubricants in phosphatidylcholine dispersions," *Soft Matter*, vol. 12, pp. 2773–2784, 2016.